

9-14-45  
9443

ADOT

TECH LIBRARY KAFB, NM  
0065963

NACA TN 3147

# NATIONAL ADVISORY COMMITTEE FOR AERONAUTICS

TECHNICAL NOTE 3147

IMPINGEMENT OF WATER DROPLETS ON AN ELLIPSOID  
WITH FINENESS RATIO 10 IN AXISYMMETRIC FLOW

By Rinaldo J. Brun and Robert G. Dorsch

Lewis Flight Propulsion Laboratory  
Cleveland, Ohio



Washington  
May 1954

AFM 6  
TECHNICAL  
AFM 28



NATIONAL ADVISORY COMMITTEE FOR AERONAUTICS

TECHNICAL NOTE 3147

IMPINGEMENT OF WATER DROPLETS ON AN ELLIPSOID WITH  
FINENESS RATIO 10 IN AXISYMMETRIC FLOW

By Rinaldo J. Brun and Robert G. Dorsch

SUMMARY

The presence of radomes and instruments that are sensitive to water films or ice formations in the nose section of all-weather aircraft and missiles necessitates a knowledge of the droplet impingement characteristics of bodies of revolution. Because it is possible to approximate many of these bodies with an ellipsoid of revolution, droplet trajectories about an ellipsoid of revolution with a fineness ratio of 10 were computed for incompressible axisymmetric air flow. From the computed droplet trajectories, the following impingement characteristics of the ellipsoid surface were obtained and are presented in terms of dimensionless parameters: (1) total rate of water impingement, (2) extent of droplet impingement zone, and (3) local rate of water impingement. These impingement characteristics are compared briefly with those previously reported for an ellipsoid of revolution with a fineness ratio of 5.

INTRODUCTION

The data presented herein are a continuation of the study reported in reference 1 on the impingement of cloud droplets on a prolate ellipsoid of revolution. The calculations discussed in reference 1 for an ellipsoid with a fineness ratio of 5 (20 percent thick) were extended for this report to an ellipsoid of fineness ratio of 10 (10 percent thick). As mentioned in the reference cited, a prolate ellipsoid of revolution is a good approximation in the determination of cloud-droplet impingement for many body shapes used for radomes, rocket pods, and bombs. The data presented herein, along with the results presented in reference 1, permit the estimation of impingement characteristics on many of these bodies.

The trajectories of atmospheric water droplets about a prolate ellipsoid of revolution with a fineness ratio of 10 moving at subsonic velocities at zero angle of attack were calculated with the aid of a differential analyzer at the NACA Lewis laboratory. From the computed

trajectories, the rate, the distribution, and surface extent of impinging water were obtained and are summarized in this report in terms of dimensionless parameters.

SYMBOLS

The following symbols are used in this report:

d	droplet diameter, microns
$E_m$	collection efficiency, dimensionless
f	fineness ratio, dimensionless
K	inertia parameter, $1.704 \times 10^{-12} d^2 U / \mu L$ , dimensionless (eq. 1)
L	major axis of ellipse, ft
$Re_0$	free-stream Reynolds number with respect to droplet, $4.813 \times 10^{-6} d_p U / \mu$ , dimensionless
r, z	cylindrical coordinates, ratio to major axis, dimensionless
$r_0$	starting ordinate at $z = -\infty$ of droplet trajectory, ratio to major axis, dimensionless
$r_{0, \tan}$	starting ordinate at $z = -\infty$ of droplet trajectory tangent to ellipsoid surface, ratio to major axis, dimensionless
S	distance along surface of ellipsoid from forward stagnation point to point of droplet impingement, ratio to major axis, dimensionless
$S_m$	limit of impingement zone, ratio to major axis, dimensionless
U	free-stream velocity, or flight-speed, mph
u	local air velocity, ratio to free-stream velocity
$W_m$	total rate of impingement of water on surface of ellipsoid, lb/hr
$W_\beta$	local rate of impingement of water, lb/(hr)(sq ft)
w	liquid-water content in cloud, g/cu m

3217

$\beta$  local impingement efficiency,  $\frac{r_0}{r} \frac{dr_0}{ds}$ , dimensionless

$\mu$  viscosity of air, slugs/(ft)(sec)

$\rho_a$  density of air, slugs/cu ft

Subscripts:

r radial component

z axial component

### CALCULATION OF DROPLET TRAJECTORIES

The equations that describe the motion of cloud droplets about an ellipsoid are given in reference 1. A solution of the differential equations of motion was obtained with the use of the mechanical analog (described in ref. 2) based on the principle of a differential analyzer. The procedure for calculating the trajectories of cloud droplets with respect to the ellipsoid of revolution with a fineness ratio of 10 (10 percent thick) is the same as that described in reference 1. As shown in figure 1, the ellipsoid orientation in the coordinate system used in reference 1 is retained herein. Since a flow field is axisymmetric around an ellipsoid of revolution oriented at  $0^\circ$  between its major axis and the direction of the free stream, the droplet impingement on the elliptical section of all meridian planes is the same, and the impingement characteristics of the ellipsoid of revolution can be obtained from trajectory calculations in the z,r plane of figure 1.

The air-flow field around the body, required for the solution of the equations, was obtained with the use of digital computers from the mathematical expressions presented in reference 1. The values of the air-velocity components  $u_z$  and  $u_r$  as functions of r and z are given in figure 2 for comparison with the flow-field velocities given in reference 1 for the 20-percent-thick ellipsoid. In figure 2(a),  $u_z$  is given as a function of z for constant values of r, while  $u_r$  as a function of r for constant z is given in figure 2(b). The velocity components in figure 2 are dimensionless, because they are ratios of the respective local velocities to the free-stream velocity; the distances r and z are also expressed as ratios of actual distance to the major axis length L.

The position of impingement of cloud droplets on the surface of the ellipsoid is given in subsequent sections in terms of the surface distance S, which is measured along the surface from the forward

2017

stagnation point. The values of  $S$  are the ratios of the actual surface distances to the major axis length  $L$ . The relation between  $S$  and  $z$  is shown in figure 3. The relation between  $S$  and  $r$  can be obtained from figure 4 from the curve for  $1/K = 0$ .

The equations of motion were solved for various values of the parameter  $1/K$  between 0.1 and 90. The inertia parameter  $K$  is a measure of the droplet size, the flight speed and size of the body of revolution, and the viscosity of the air, through the relation

$$K = 1.704 \times 10^{-12} d^2 U / \mu L \quad (1)$$

The density of water and the acceleration of gravity, which are expressed as part of the conversion factor, are 62.4 pounds per cubic foot and 32.17 feet per second per second, respectively. For each value of the parameter  $1/K$ , a series of trajectories was computed for each of several values of free-stream Reynolds number  $Re_0$ : 0, 128, 512, 1024, 4096, and 8192. The free-stream Reynolds number is defined with respect to the droplet size as

$$Re_0 = 4.813 \times 10^{-6} d_p U / \mu \quad (2)$$

In order that these dimensionless parameters have more physical significance in the following discussion, some typical combinations of  $K$  and  $Re_0$  are presented in table I in terms of the length and velocity of the ellipsoid, the droplet size, and the flight pressure altitude and temperature. Equations and graphical procedure for translating the dimensionless parameters used in this report into terms of flight speed, major axis length, altitude, and droplet size are presented in appendix B of reference 3.

### RESULTS AND DISCUSSION

The results of the calculation of droplet trajectories about the ellipsoid of revolution of fineness ratio 10 (10 percent thick) at zero angle of attack are summarized in figure 4, where the starting ordinate at infinity  $r_0$  of each trajectory is given as a function of the point of impingement on the surface in terms of  $S$ . Each of the solid lines, except for  $1/K = 0$ , is obtained from a series of calculated trajectories. The curve for  $1/K = 0$  is obtained from the mathematical relation between  $S$  and  $r$  for an ellipse. The dashed lines in figure 4 are the loci of the termini of the constant  $1/K$  curves. As was the case for the ellipsoid with a fineness ratio of 5 (ref. 1), these loci were found to be the same within the order of accuracy of the computations for all values of  $Re_0$  (figs. 4(a) to (f)). From the data presented

3217

in this figure, the rate, the area, and the distribution of water-droplet impingement on the surface of the ellipsoid can be determined for given values of  $Re_0$  and  $K$ .

### Total Rate of Impingement of Water

In flight through clouds composed of droplets of uniform size, the total amount of water in droplet form impinging on the ellipsoid is determined by the amount of water contained in the volume within the envelope of tangent trajectories (fig. 1). The total rate of impingement of water (lb/hr) can be determined from the following relation derived in reference 1:

$$W_m = 1.04 r_{0,tan}^2 w L^2 U \quad (3)$$

where the flight speed  $U$  is in miles per hour, the liquid-water content  $w$  is in grams per cubic meter, and  $L$  is in feet.

The value of  $r_{0,tan}$  for a given combination of  $Re_0$  and  $K$  can be obtained from figure 4 by determining the value of  $r_0$  that corresponds to the maximum  $S (S_m)$  for the constant  $K$  curve of interest. The values of  $r_{0,tan}$  fall on the dashed termini curves of figure 4. In order to facilitate interpolation and extrapolation, the data are replotted in the form of  $r_{0,tan}^2$  as a function of  $K$  for constant  $Re_0$  in figure 5.

The accuracy in the determination of  $r_{0,tan}$  from the calculated trajectories is about the same for the 10-percent-thick ellipsoid as for the 20-percent-thick ellipsoid discussed in reference 1. For values of  $r_{0,tan}$  greater than 0.015,  $r_{0,tan}$  was determined with an accuracy of the order of  $\pm 0.0003$ . For combinations of  $1/K$  and  $Re_0$  that result in values of  $r_{0,tan}$  between 0.015 and 0.01, the accuracy of  $r_{0,tan}$  is within  $\pm 0.0007$ . For reported values of  $r_{0,tan} < 0.01$ , the accuracy in determining the tangent trajectory is somewhat indefinite, but appears to be within  $\pm 0.001$ .

The effect of body size on the value of  $r_{0,tan}^2$  for selected cloud-droplet sizes and flight conditions is illustrated in figure 6. The calculated values given in figure 6 are for ellipsoids with a fineness ratio of 10 and major axis lengths between 3 and 300 feet, for flight at 50, 100, 300, or 500 miles per hour through uniform clouds composed of droplets of 10, 20, or 50 microns in diameter. Pressure altitudes of 5,000, 15,000, and 25,000 feet, and temperatures (most probable icing

3217

temperature given in ref. 3) of 20°, 1°, and -25° F, respectively, were used for the calculations. For example, consider a 40-foot-long ellipsoid with a fineness ratio of 10 moving at 500 miles per hour at zero angle of attack at a pressure altitude of 15,000 feet through a uniform cloud composed of droplets 20 microns in diameter. From figure 6(b),  $r_{0,tan}^2$  is 0.000056. If the liquid-water content of the cloud is assumed to be 0.1 gram per cubic meter, then (from eq. (3)) the total rate of impingement of water  $W_m$  is 4.7 pounds per hour.

3217

#### Extent of Droplet Impingement Zone

The extent of the droplet impingement zone on the surface of the ellipsoid is obtained from the tangent trajectories (fig. 1). The point of tangency determines the rearward limit of the impingement zone. The limit of impingement  $S_m$  for a particular  $Re_0$  and  $K$  condition can be determined from the maximum  $S$  value of the constant  $K$  curves of interest in figure 4. Again, to facilitate interpolation, the data are replotted in the form of  $S_m$  as a function of  $K$  for constant  $Re_0$  values in figure 7. The data of this figure indicate that the maximum extent of impingement increases with increasing  $K$  but decreases with increasing  $Re_0$ .

Because of the difficulty in determining the exact point of tangency on the surface of the ellipsoid of each tangent trajectory, the accuracy in determining  $S_m$  is of the order of  $\pm 0.005$ . The accuracy in determining the value of  $S$  for the intermediate points of impingement (between  $S_m$  and forward stagnation point) given in figure 4 was much higher, because the points at which the intermediate trajectories terminated on the ellipsoid surface were much better defined.

The effect of body size on the value of  $S_m$  for selected cloud-droplet and flight conditions is illustrated in figure 8. For example, consider a 20-foot-long ellipsoid with a fineness ratio of 10 moving 300 miles per hour at zero angle of attack at a 5000-foot pressure altitude through a uniform cloud composed of 50-micron droplets. From figure 8(a),  $S_m$  is 0.102; that is, the impingement zone extends 2.04 feet rearward (measured along the surface) from the forward stagnation point.

#### Local Rate of Impingement of Water

The local rate of impingement of water in droplet form (lb/(hr)(sq ft)) on the surface of the ellipsoid can be determined from the expression



$$W_{\beta} = 0.33 U_w \frac{r_0}{r} \frac{dr_0}{dS} = 0.33 U_w \beta \quad (4)$$

where  $\beta$  is the local impingement efficiency. The values of  $\beta$  as a function of  $S$  for combinations of  $Re_0$  and  $K$  are presented in figure 9. These curves were obtained by multiplying the slope of the curves in figure 4 by the corresponding ratio  $r_0/r$  at each point. Because the slopes of the curves of  $r_0$  as a function of  $S$  (fig. 4) in the region between  $S = 0$  and  $S = 0.01$  are difficult to determine, the exact values of  $\beta$  between  $S = 0$  and  $S = 0.01$  are not known. The dashed portions of the  $\beta$  curves are extrapolations that were maintained consistent with a seemingly reasonable pattern.

#### Comparison of 10- and 20-Percent-Thick Ellipsoids

Collection efficiency. - The collection efficiency of an ellipsoid is defined as the ratio of the actual amount of water intercepted by the ellipsoid to the total amount of water in droplet form contained in the volume swept out by the ellipsoid. In terms of the ellipsoid fineness ratio  $f$  and  $r_{0,tan}^2$ , the collection efficiency may be defined as

$$E_m = 4r_{0,tan}^2 f^2 \quad (5)$$

For the 10-percent-thick ellipsoid ( $f = 10$ ), the collection efficiency may be obtained from the curves of figure 5 through the expression  $E_m = 400 r_{0,tan}^2$ . The results of the application of this equation to the data of figure 5 are shown in figure 10(a). Some curves for the collection efficiency of a 20-percent-thick ellipsoid ( $f = 5$ ) are also shown in figure 10(a) for comparison with those for the thinner body. The values of collection efficiency for the 20-percent-thick ellipsoid were obtained from figure 6 of reference 1 through the relation

$$E_m = 100 r_{0,tan}^2$$

A comparison of the collection efficiency for the two fineness ratios indicates that the collection efficiency for the two ellipsoids is nearly the same for  $Re_0 = 0$ , except for small and large values of  $K$ . For large values of  $Re_0$ , the collection efficiency of the 10-percent-thick ellipsoid is greater than that of the 20-percent-thick ellipsoid. The effect of differences in collection efficiency on the rate of impingement is best discussed after the total rates of impingement of water have been examined.

3217



Total rate of impingement of water. - For a given set of atmospheric and flight conditions and a major axis length  $L$ , the rate of water impingement is proportional to  $r_{0,\tan}^2$  (eq. (3)). A comparison of the rate of water impingement (given as  $r_{0,\tan}^2$ ) is made in table I between the two ellipsoids of different fineness ratio. The data for the ellipsoid with a fineness ratio of 5 are obtained from table I of reference 1; whereas, the results for the ellipsoid with a fineness ratio of 10 are obtained from figure 5 of this report.

The results presented in table I show that, under all comparable flight and atmospheric conditions, the rate of water impingement is less on the thinner ellipsoid (major axes of two ellipsoids are the same). The difference in rate of impingement between the two ellipsoids is much larger under combinations of flight and atmospheric conditions resulting in high rates of impingement than under conditions in which the impingement is limited to a region around the stagnation point. For example: at an altitude of 5000 feet, a speed of 500 miles per hour, and in a cloud composed of droplets 50 microns in diameter, a 20-percent-thick ellipsoid with a major axis of 3 feet would be subjected to a rate of water impingement of over 3.7 times the rate of impingement on a 10-percent-thick ellipsoid under the same conditions; whereas, if the flight speed is reduced to 50 miles per hour and the droplet diameter to 10 microns, the same 20-percent-thick ellipsoid would be subjected to only 1.2 times the rate of impingement intercepted by a 10-percent-thick ellipsoid of the same length.

The use of collection efficiency in comparing impingement characteristics of aerodynamic bodies is very often misleading, as shown by an example. The collection efficiency of a 3-foot ellipsoid moving 500 miles per hour at a 5000-foot altitude through a cloud composed of 50-micron droplets is 0.636 (fig. 6(a) and eq. (5)) for the 10-percent-thick ellipsoid as compared with 0.590 for the 20-percent-thick ellipsoid (ref. 1). Although the collection efficiency for the thinner ellipsoid is 1.08 times that for the ellipsoid with twice the diameter (major axes same), the thicker body was shown in the preceding paragraph to intercept over 3.7 times as much water under these same atmospheric and flight conditions. This example illustrates the need to account for the differences in the projected frontal area of the bodies when the concept of collection efficiency is used in comparing the impingement characteristics of two ellipsoids.

Surface extent. - The surface extent of impingement is compared in figure 10(b) for the two ellipsoids by comparing some curves of  $S_m$  given in figure 7 with curves for equivalent conditions for the 20-percent-thick ellipsoid presented in figure 8 of reference 1. The curves for low values of  $Re_0$  are very nearly coincident. For large values of

3217

$Re_0$ , the rearward limit of impingement is slightly greater on the 10-percent-thick ellipsoid. In terms of usual flight and atmospheric conditions, this means that the rearward extent of impingement is somewhat greater for the thinner ellipsoid when flying through rain or drizzle (table I), but is very nearly the same when cloud droplets are encountered.

3217  
Nonuniform droplet size. - The data presented in all the figures and discussion are based on flights in clouds composed of droplets that are all uniform in size. As was shown in reference 1, the total rate of water impingement when a distribution of droplet sizes is assumed may be different from that obtained on the basis of the volume-median size only. A comparison of the total rate of impingement is made here between the 10-percent-thick ellipsoid and the 20-percent-thick ellipsoid, using the droplet-size distribution given in figure 11 of reference 1 and the computational procedure described in that reference. The volume-median droplet size is again assumed to be 20 microns, the velocity 200 miles per hour, the ellipsoid length 10 feet, the pressure altitude 5000 feet, and the temperature 20° F. On a weighted basis and for the particular droplet-size distribution assumed (fig. 11, ref. 1), the thicker ellipsoid intercepts about 3.1 times as much water. On a volume-median basis (wherein a uniform droplet size equal to the volume-median droplet size of the distribution is assumed), the thicker ellipsoid intercepts 2.8 times as much water.

#### CONCLUDING REMARKS

Because the droplet trajectories about the ellipsoid were calculated for incompressible fluid flow, a question may arise as to their applicability at the higher subsonic flight speeds. As was discussed in reference 1, the ellipsoid impingement results should be applicable for most engineering uses throughout the subsonic region (also see ref. 4).

The data of this report apply directly only to ellipsoids of revolution with a fineness ratio of 10. The cautions presented in reference 1 regarding the extension of the data presented in that report for the 20-percent-thick ellipsoid to bodies of other shapes are reemphasized here. In some cases, where the body is of different shape, it may be possible to match its nose section physically with the section of an ellipsoid of selected length and fineness ratio for which data are available herein or in reference 1. If, in such a case, the contribution of the afterbody to the air-flow field in the vicinity of the nose of the body is small (as it often is), then the impingement data for the matching portion of the surface of the ellipsoid can be used for determining the impingement characteristics of the nose region of the body. In other

cases, where the body shape differs from that of an ellipsoid but the fineness ratio is the same, the air-flow field may be similar enough that an estimate of the total catch can be obtained from the ellipsoid data. In this case, no details of the surface distribution of impinging water could be obtained.

Lewis Flight Propulsion Laboratory  
National Advisory Committee for Aeronautics  
Cleveland, Ohio, February 25, 1954

#### REFERENCES

1. Dorsch, Robert G., Brun, Rinaldo J., and Gregg, John L.: Impingement of Water Droplets on an Ellipsoid with Fineness Ratio 5 in Axisymmetric Flow. NACA TN 3099, 1954.
2. Brun, Rinaldo J., and Mergler, Harry W.: Impingement of Water Droplets on a Cylinder in an Incompressible Flow Field and Evaluation of Rotating Multicylinder Method for Measurement of Droplet-Size Distribution, Volume-Median Droplet Size, and Liquid-Water Content in Clouds. NACA TN 2904, 1953.
3. Brun, Rinaldo J., Gallagher, Helen M., and Vogt, Dorothea E.: Impingement of Water Droplets on NACA 65<sub>1</sub>-208 and 65<sub>1</sub>-212 Airfoils at 4° Angle of Attack. NACA TN 2952, 1953.
4. Brun, Rinaldo J., Serafini, John S., and Gallagher, Helen M.: Impingement of Cloud Droplets on Aerodynamic Bodies as Affected by Compressibility of Air Flow Around the Body. NACA TN 2903, 1953.

TABLE I. - RELATION OF DIMENSIONLESS PARAMETERS TO BODY SIZE AND ATMOSPHERIC AND FLIGHT CONDITIONS

Pressure altitude, ft Temperature, °F Viscosity of air, $\mu$ , slugs/(ft)(sec) Density of air, $\rho_a$ , slugs/cu ft				8000 80 $3.487 \times 10^{-7}$ 0.002155								25,000 -25 $3.230 \times 10^{-7}$ 0.001080							
				Re <sub>0</sub>	K	1/K	10-Percent ellipsoid		20-Percent ellipsoid		Re <sub>0</sub>	K	1/K	10-Percent ellipsoid		20-Percent ellipsoid			
$r_{0,tan}^2$ (fig. 5)	$s_m$ (fig. 7)	$r_{0,tan}^2$ (fig. 5)	$s_m$ (fig. 7)				$r_{0,tan}^2$ (fig. 5)	$s_m$ (fig. 7)	$r_{0,tan}^2$ (fig. 5)	$s_m$ (fig. 7)									
Atmospheric condition	Ellipsoid velocity, U, mph	Droplet diameter, d, microns	Major axis, L, ft																
Cloud droplets	50	10	3	14.7	0.008125	123.1	0.00005	0.019	0.00006	0.017	7.858	0.008795	113.7	0.00005	0.090	0.00006	0.018		
			50	14.7	.0008125	1231	0	.001	0	0	7.858	.0008795	1137	0	.001	0	0		
			100	14.7	.0002437	4103	0	0	0	0	7.858	.0002437	3791	0	0	0	0		
	50	3	75.54	0.2051	4.294	0.00059	0.161	0.00224	0.165	59.17	0.2198	4.550	0.00076	0.193	0.00272	0.199			
			50	.02051	46.24	.00006	.027	.00012	.054	59.17	.02198	45.50	.00008	.032	.00021	.042			
			100	.008092	164.1	.00002	.013	.00002	.012	59.17	.008394	151.7	.00003	.016	.00003	.013			
	100	20	10	58.81	0.01949	51.51	0.00007	0.029	0.00014	0.038	31.34	0.02110	47.39	0.00008	0.051	0.00021	0.043		
			50	58.81	.003899	256.5	.00001	.010	.00001	.007	31.34	.00422	237.0	.00002	.011	.00002	.008		
			300	58.81	.0008497	1539	0	0	0	0	31.34	.0007033	1422	0	0	0			
	300	10	10	178.4	0.05845	17.11	0.00014	0.048	0.00042	0.080	84.00	0.06350	15.8	0.00018	0.080	0.00082	0.071		
			50	178.4	.01189	85.54	.00002	.017	.00002	.019	84.00	.01268	78.99	.00004	.020	.00004	.023		
			100	88.2	.001452	884.0	0	.004	0	0	47.01	.001583	831.7	.00001	.004	.00001	.001		
200			178.4	.005848	171.1	.00001	.012	.00001	.009	84.00	.008330	156.0	.00002	.014	.00002	.012			
300			178.4	.001949	513.1	.00001	.004	.00001	.001	84.00	.002110	473.9	.00001	.008	.00001	.002			
500	20	10	294.1	0.09745	10.26	0.00021	0.058	0.00075	0.078	158.7	0.1085	9.479	0.00027	0.085	0.00095	0.080			
		50	294.1	.01949	51.51	.00004	.021	.00007	.027	158.7	.02110	47.39	.00005	.028	.00008	.030			
		100	294.1	.00745	102.8	.00001	.018	.00001	.016	158.7	.01055	94.79	.00001	.017	.00001	.017			
	50	3	755.4	2.051	0.4924	0.00159	0.385	0.00590	0.351	391.7	2.198	0.4550	0.00182	0.398	0.00880	0.392			
			50	.2051	4.924	.00029	.098	.00100	.098	391.7	.2198	4.550	.00041	.116	.00154	.125			
			100	.08092	16.41	.00008	.032	.00024	.043	391.7	.08594	15.17	.00012	.042	.00041	.054			
Drizzle	100	400	10	1178	7.788	0.1263	0.00214	0.452	0.00840	0.448	626.7	8.442	0.1185	0.00225	0.471	0.00886	0.488		
			300	5529	2.559	.4275	.00112	.275	.00377	.247	1880	2.592	.3949	.0019	.332	.00553	.513		
			500	5529	.7797	1.293	.00045	.134	.00132	.113	1880	.8440	1.185	.00068	.188	.00253	.180		
			500	5882	1.299	.7698	.00056	.153	.00178	.158	3134	1.407	.7107	.00082	.215	.00278	.202		
Rain	300	1000	50	8823	29.24	0.0342	0.00217	0.482	0.00832	0.446	4701	31.88	0.03159	0.00229	0.475	0.00896	0.486		
			100	8823	14.62	.0684	.00195	.422	.00702	.390	4701	15.83	.08317	.00214	.462	.00813	.435		
			300	8823	4.873	.2052	.00117	.292	.00368	.283	4701	5.277	.1895	.00180	.368	.00550	.325		

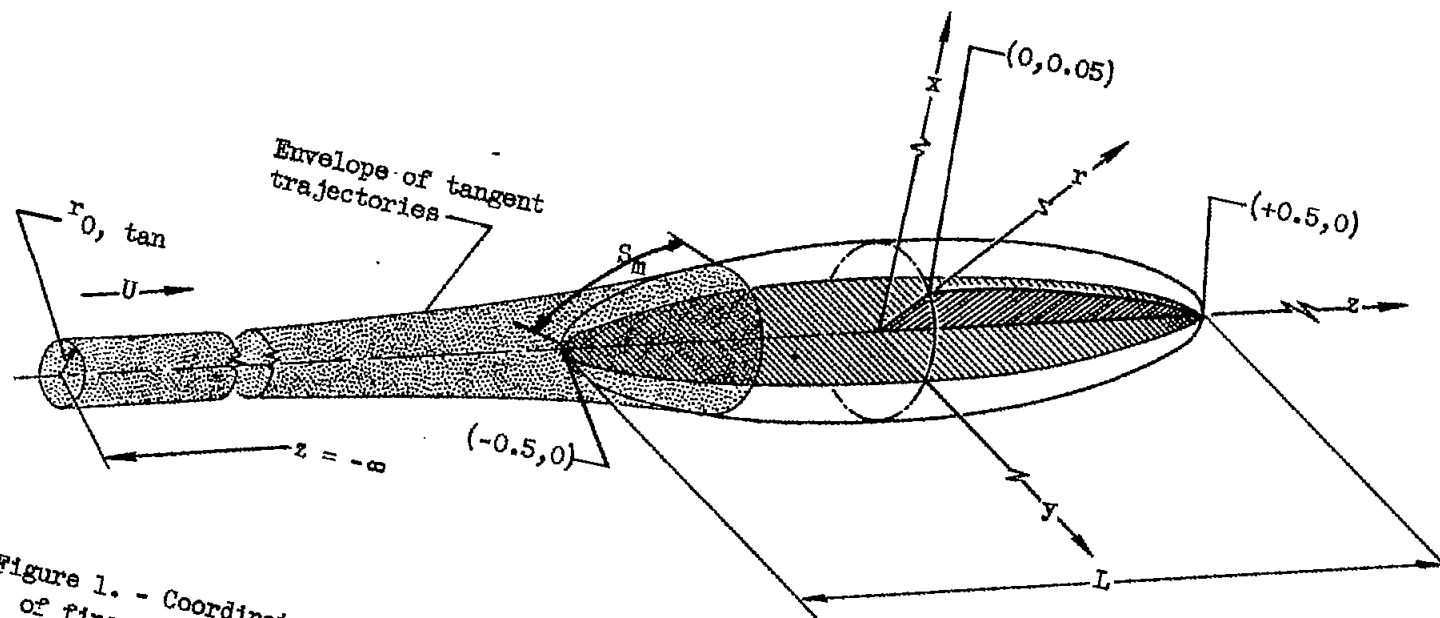
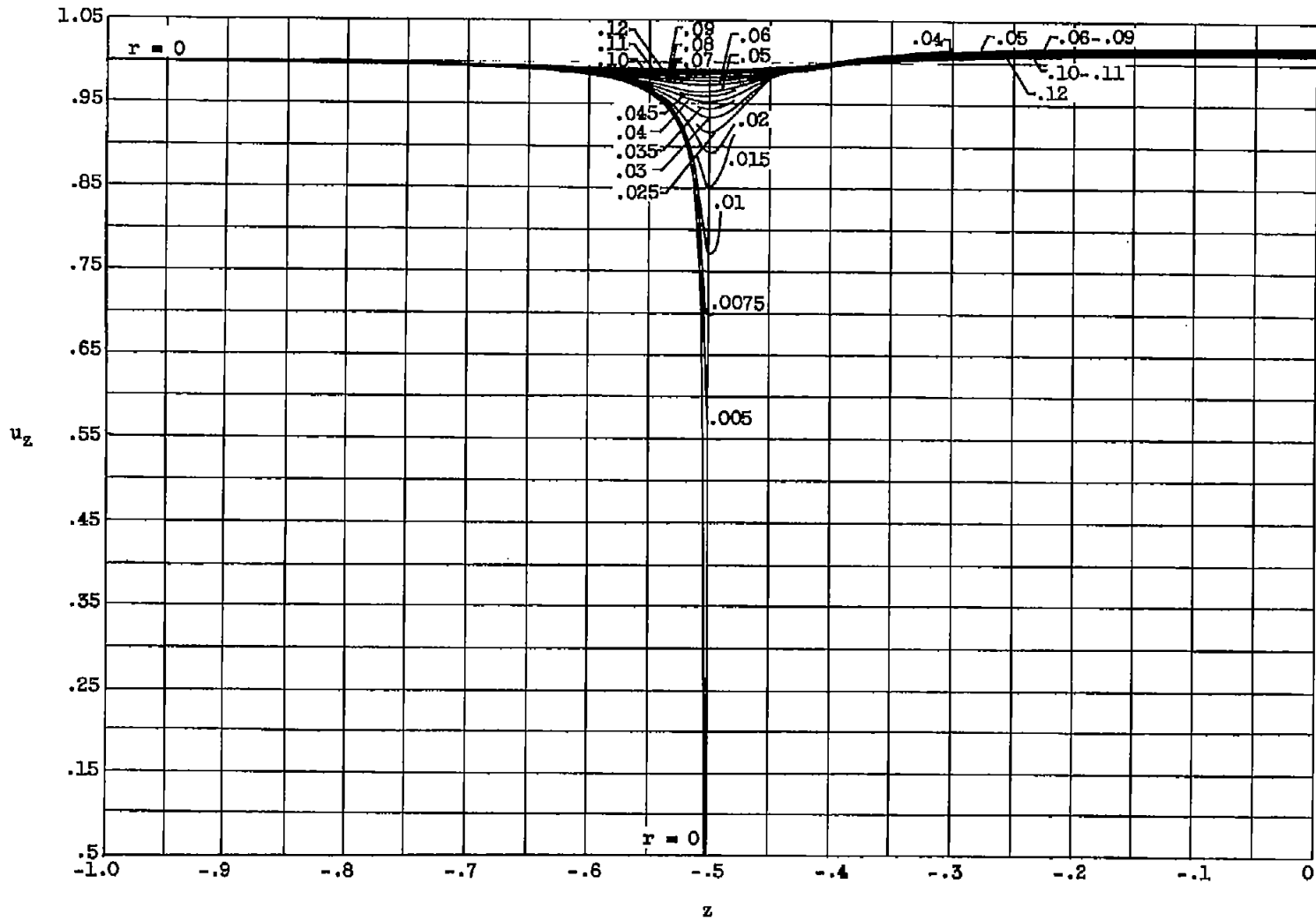


Figure 1. - Coordinate system for droplet trajectory calculations about an ellipsoid of revolution of fineness ratio 10.

CD-3431

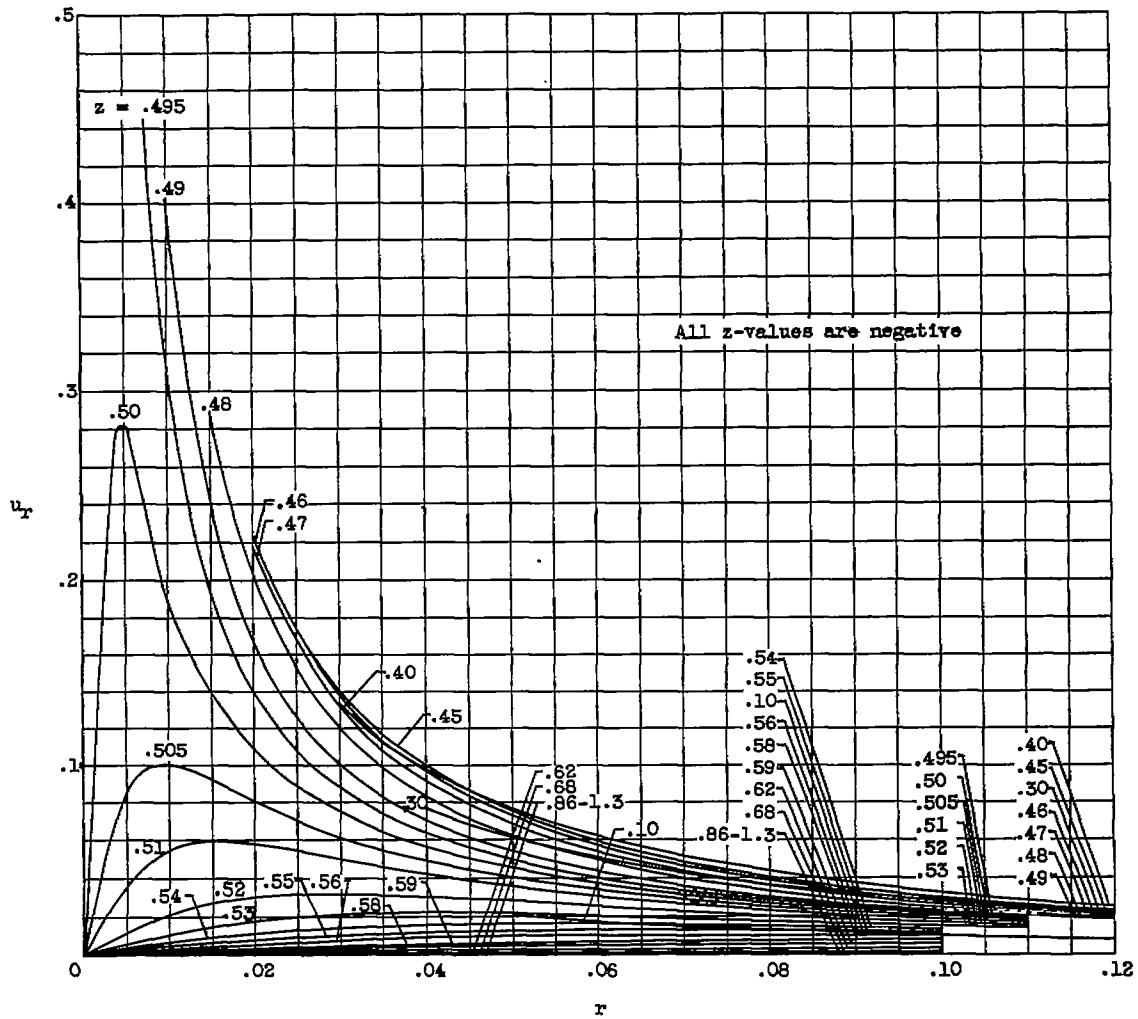
NACA TM 3147

1720



(a) z-Component of air velocity as function of  $z$  for constant values of  $r$ .

Figure 2. - Flow field for 10-percent-thick ellipsoid.



(b) r-Component of air velocity as function of  $r$  for constant values of  $z$ .

Figure 2. - Concluded. Flow field for 10-percent-thick ellipsoid.

3217



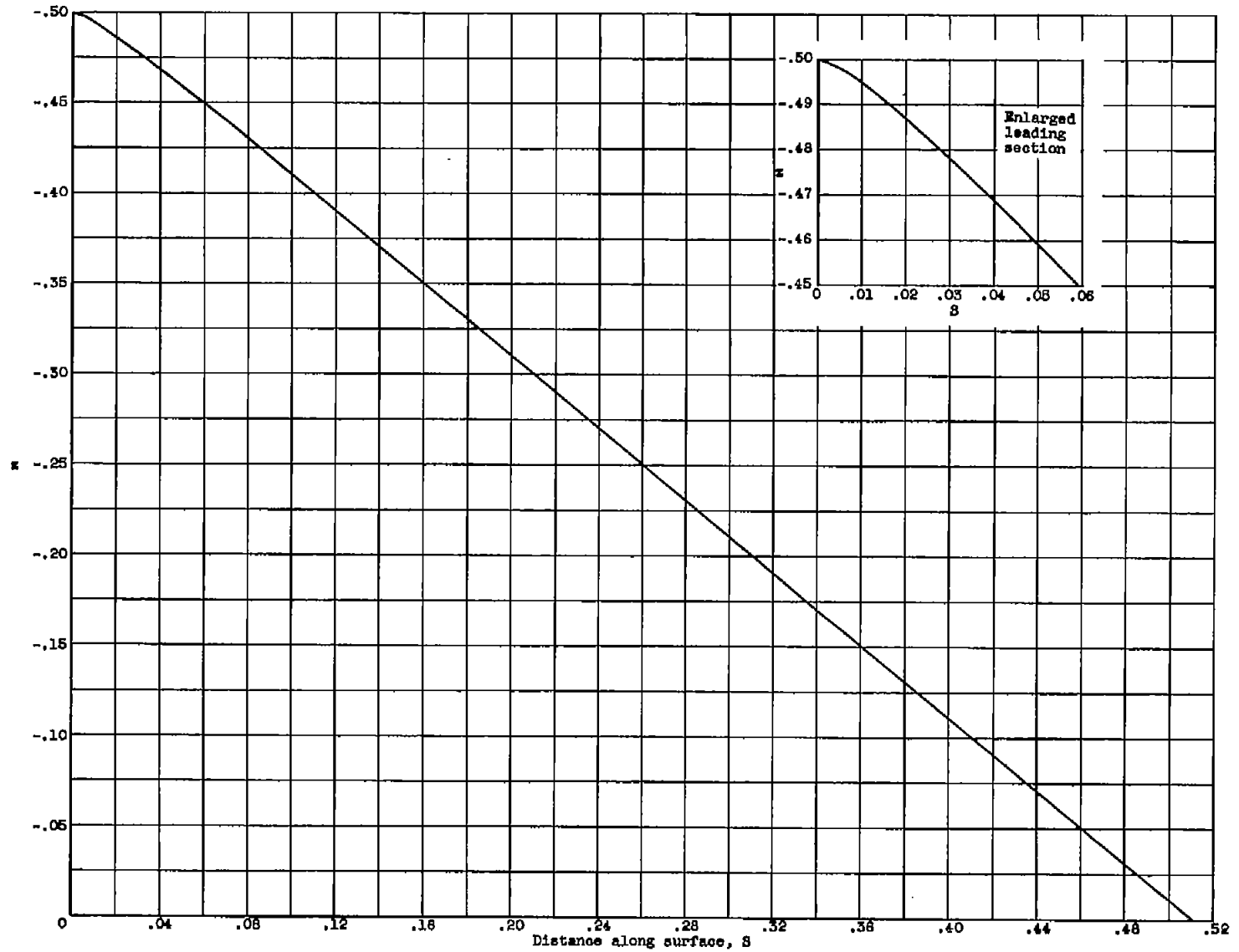
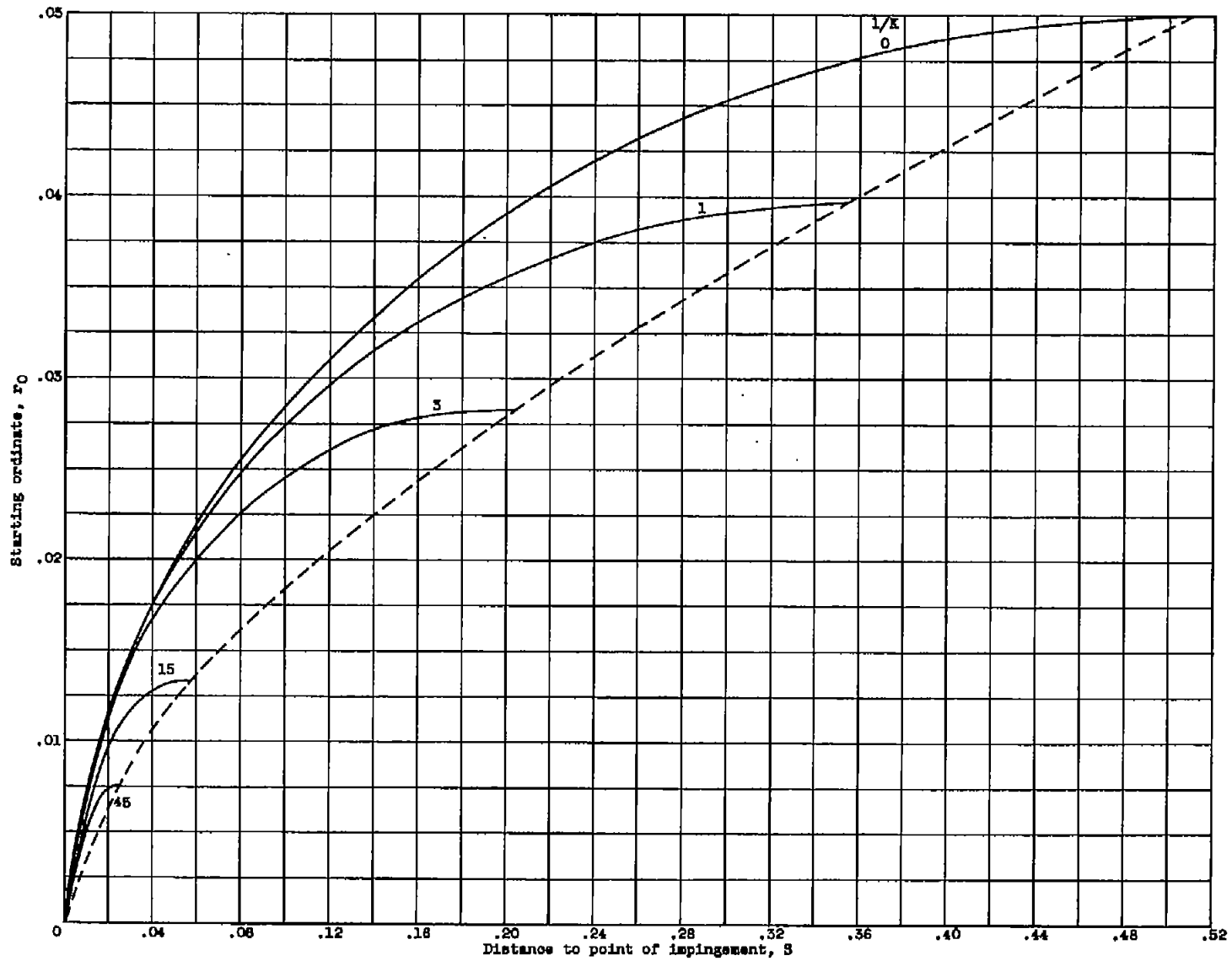


Figure 3. - Relation between distance along ellipsoid surface and z-coordinate.



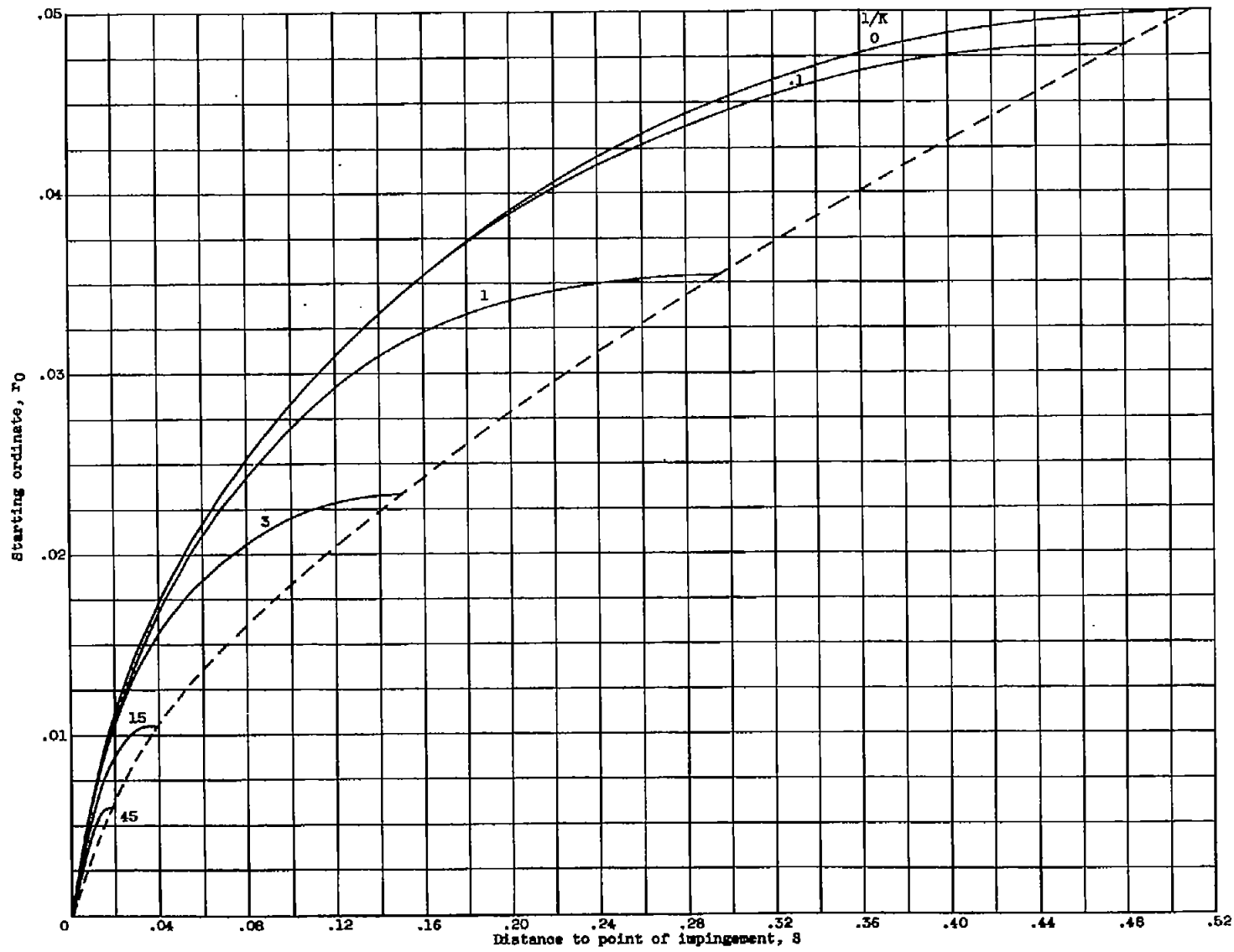
(a) Free-stream Reynolds number, 0.

Figure 4. - Starting ordinate as function of distance along surface to point of impingement.



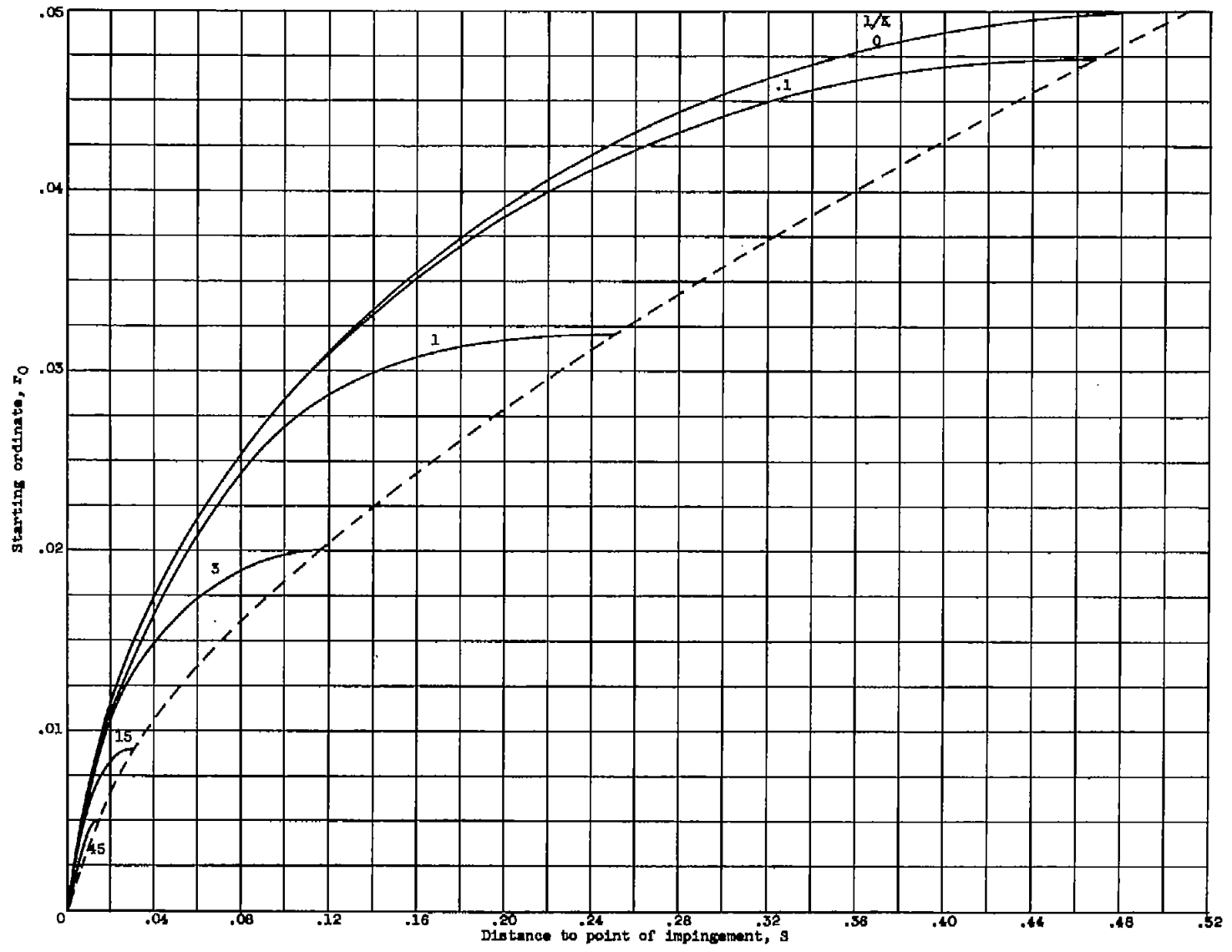
(b) Free-stream Reynolds number, 128.

Figure 4. - Continued. Starting ordinate as function of distance along surface to point of impingement.



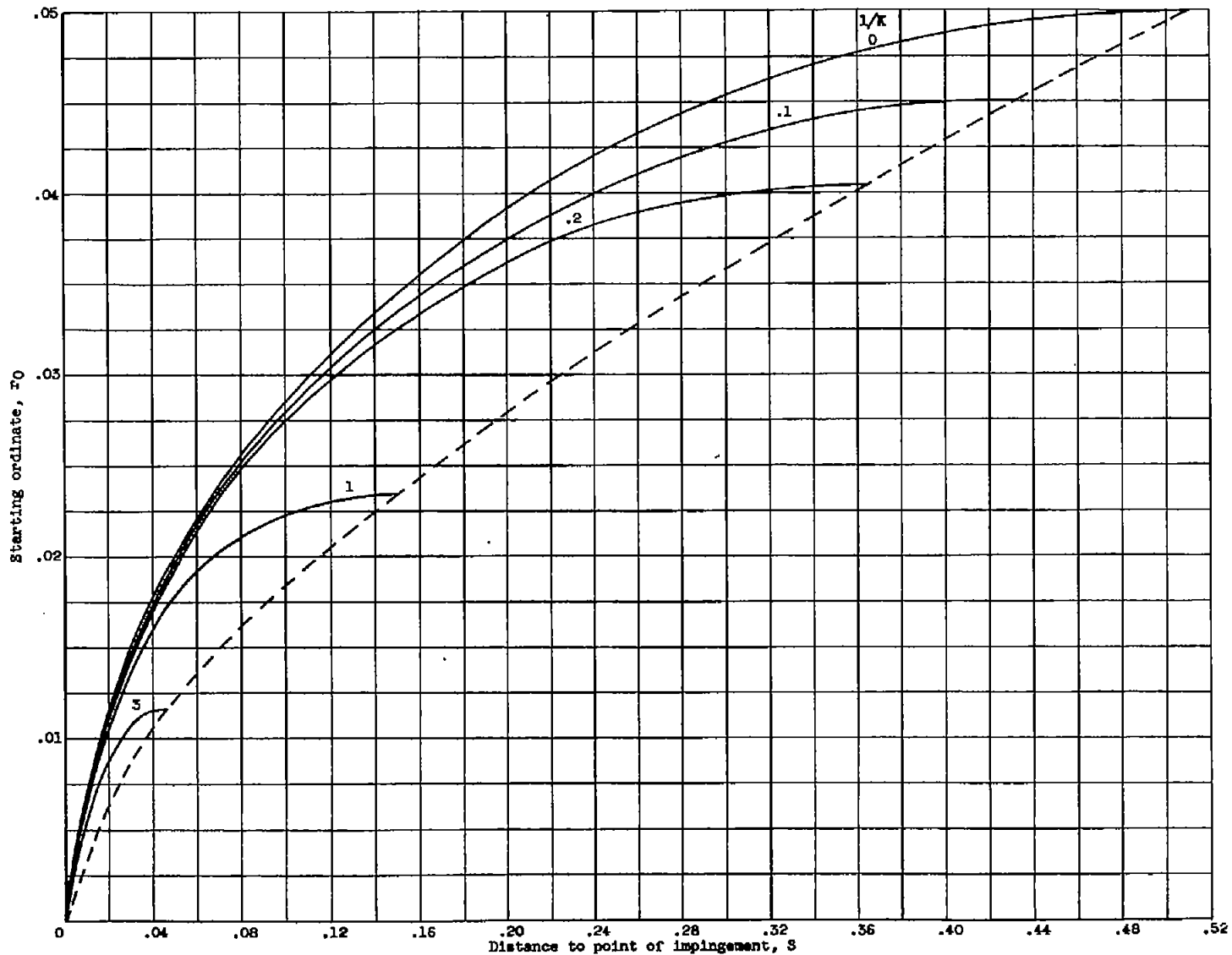
(c) Free-stream Reynolds number, 512.

Figure 4. - Continued. Starting ordinate as function of distance along surface to point of impingement.



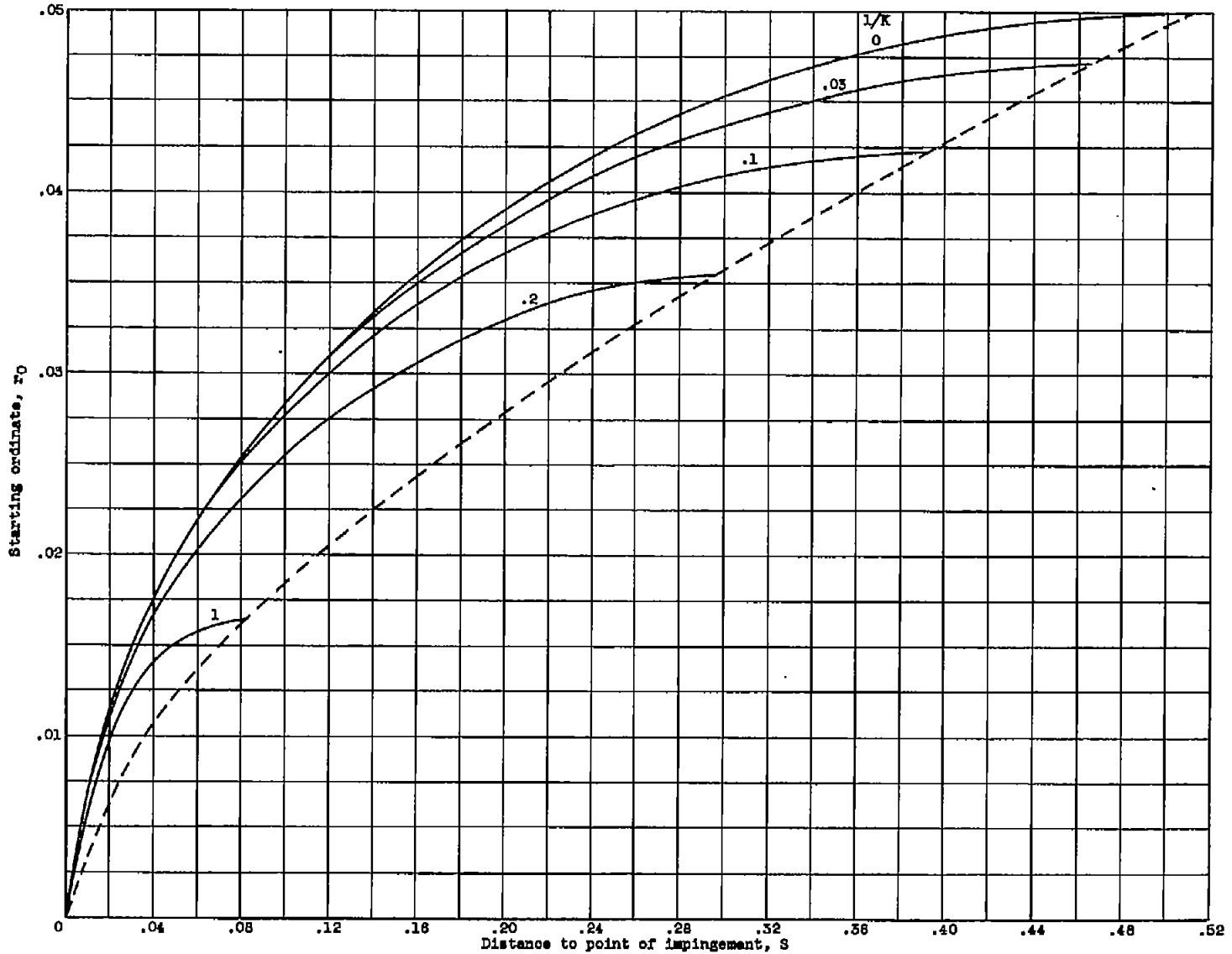
(d) Free-stream Reynolds number, 1024.

Figure 4. - Continued. Starting ordinate as function of distance along surface to point of impingement.



(e) Free-stream Reynolds number, 4096.

Figure 4. - Continued. Starting ordinate as function of distance along surface to point of impingement.



(f) Free-stream Reynolds number, 8192.

Figure 4. - Concluded. Starting ordinate as function of distance along surface to point of impingement.



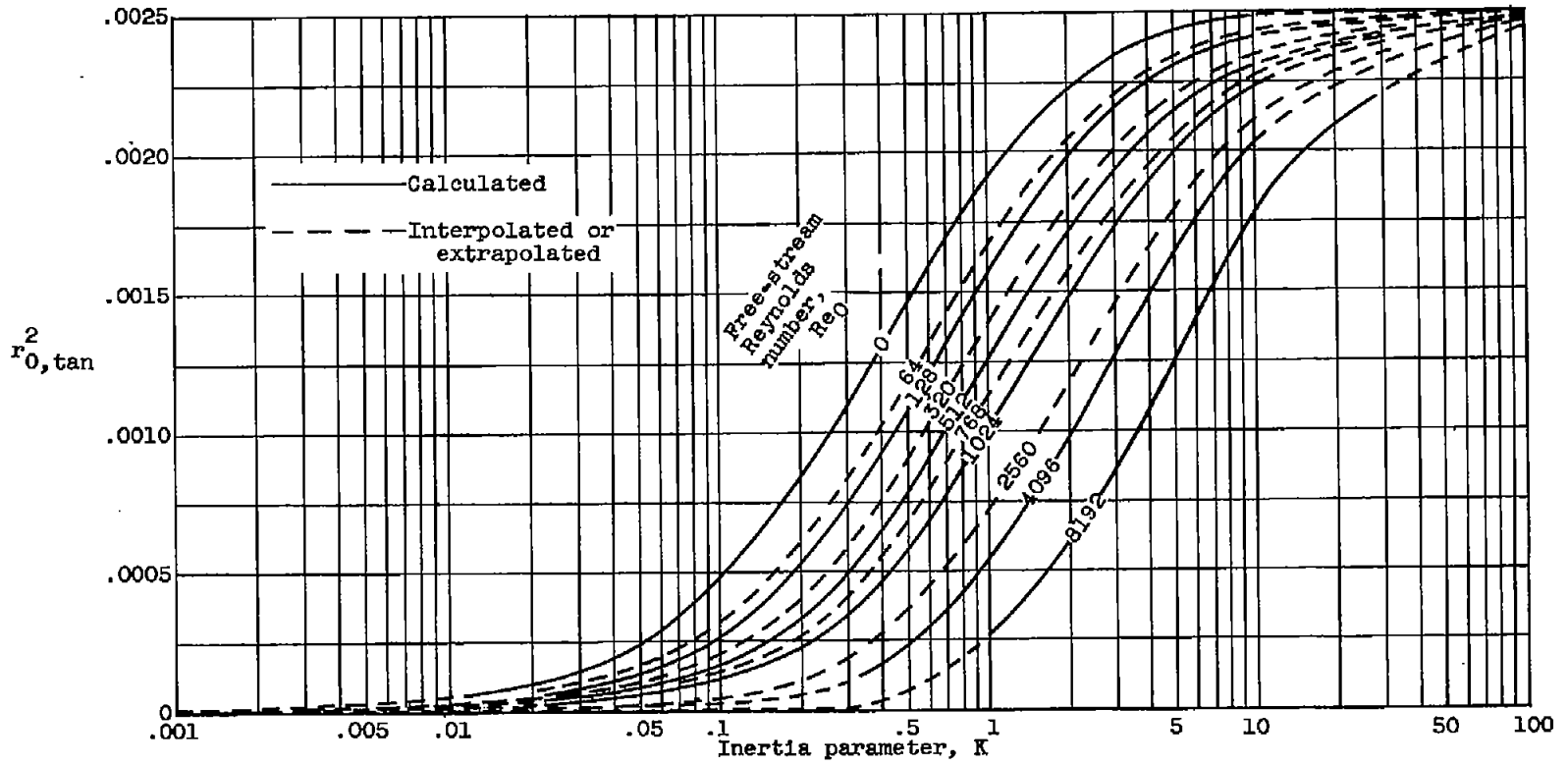
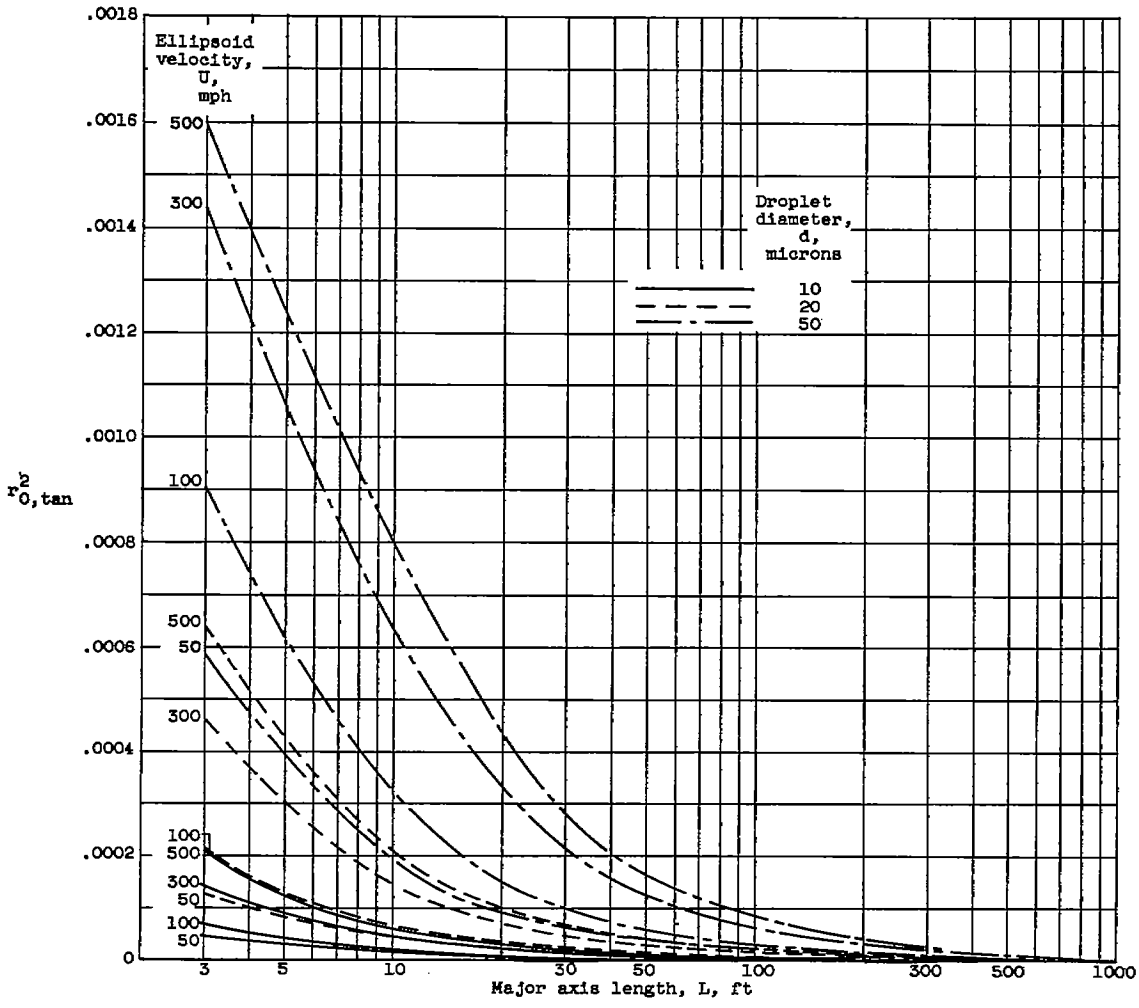


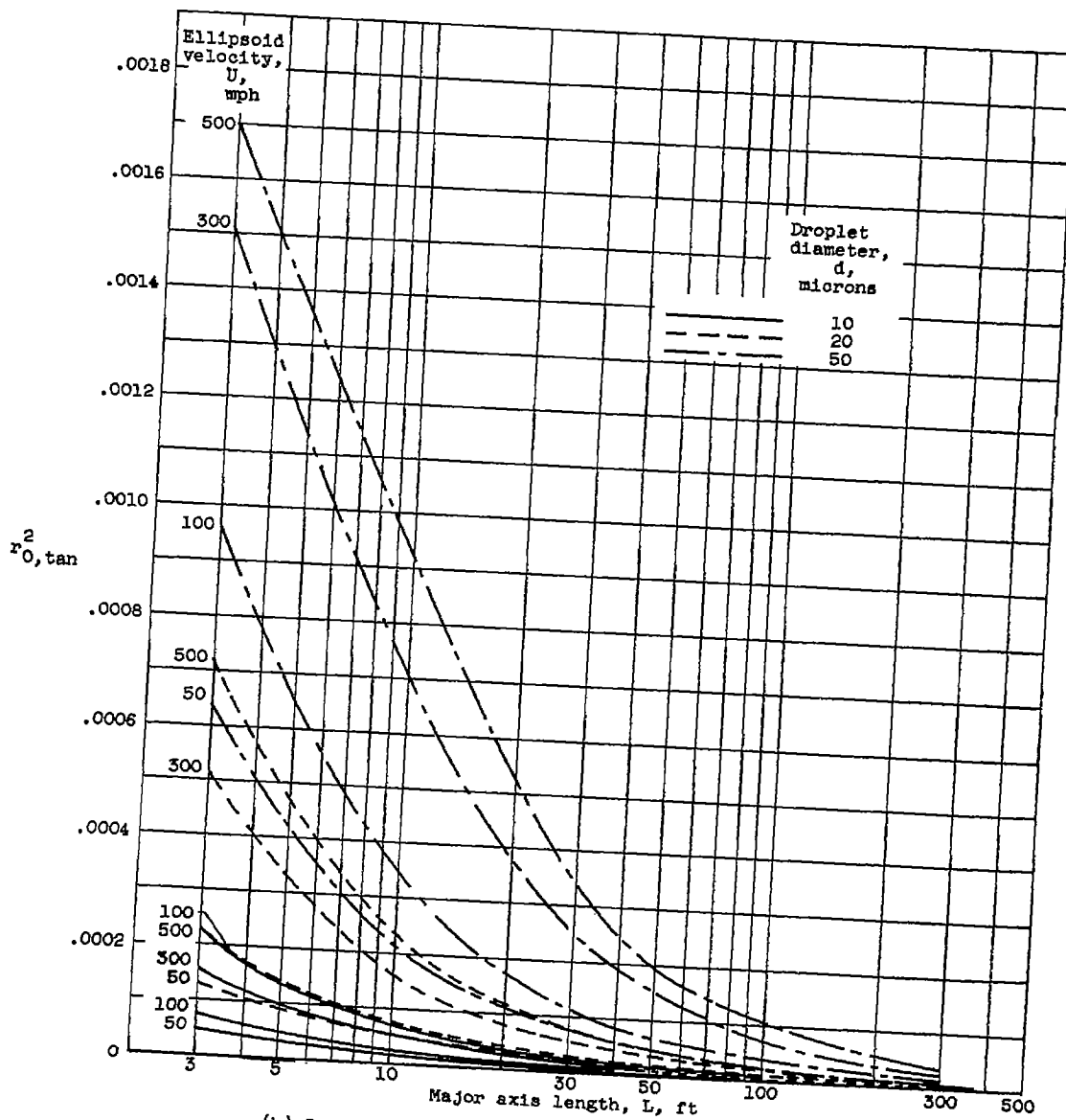
Figure 5. - Square of starting ordinate of tangent trajectory as function of inertia parameter.



(a) Pressure altitude, 5000 feet; temperature, 20° F.

Figure 6. - Square of starting ordinate of tangent trajectory as function of major axis length of ellipsoid.

1770



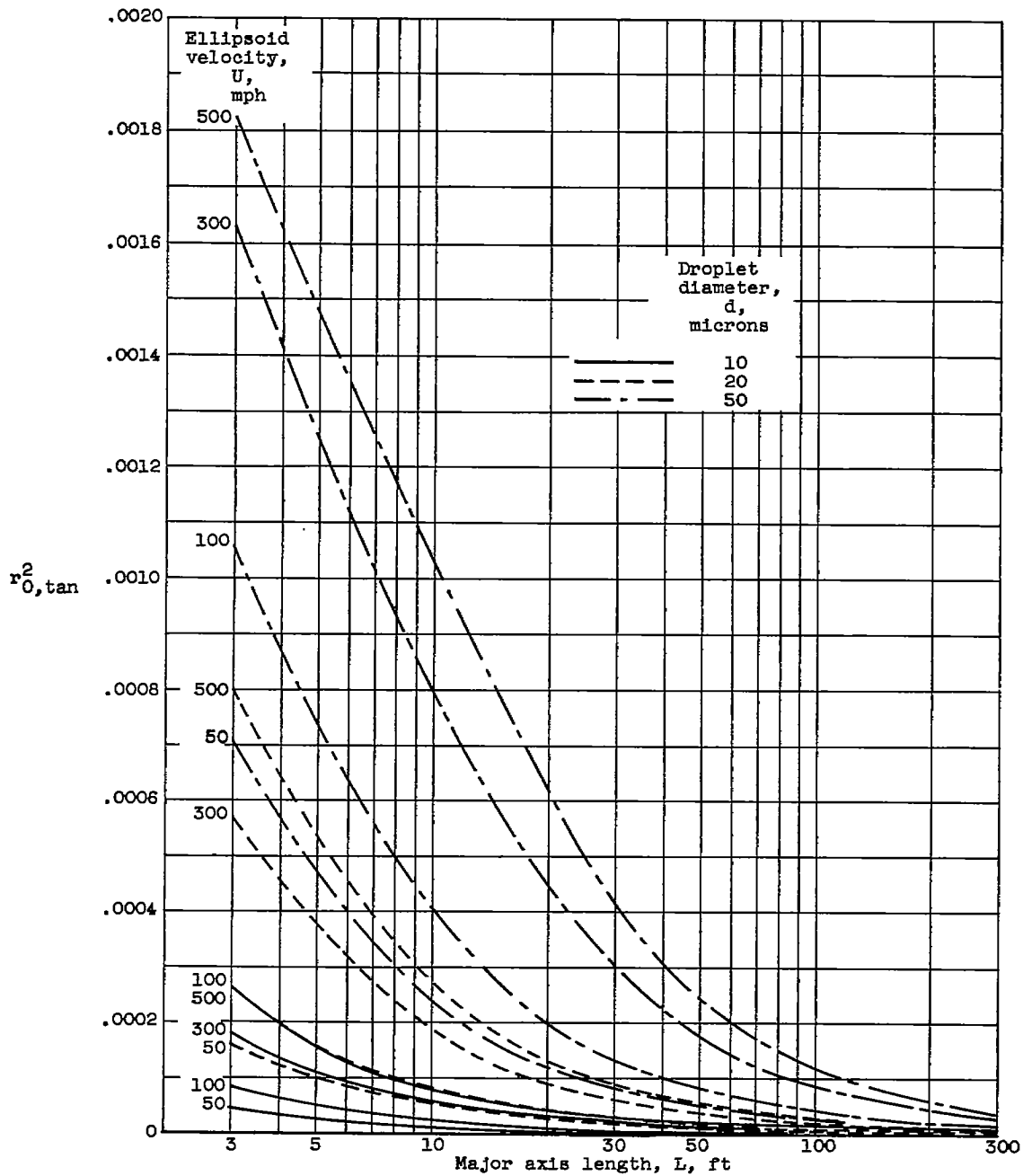
(b) Pressure altitude, 15,000 feet; temperature, 1° F.

Figure 6. - Continued. Square of starting ordinate of tangent trajectory as function of major axis length of ellipsoid.

3217

3217

CJ-4



(c) Pressure altitude, 25,000 feet; temperature, -25° F.

Figure 6. - Concluded. Square of starting ordinate of tangent trajectory as function of major axis length of ellipsoid.

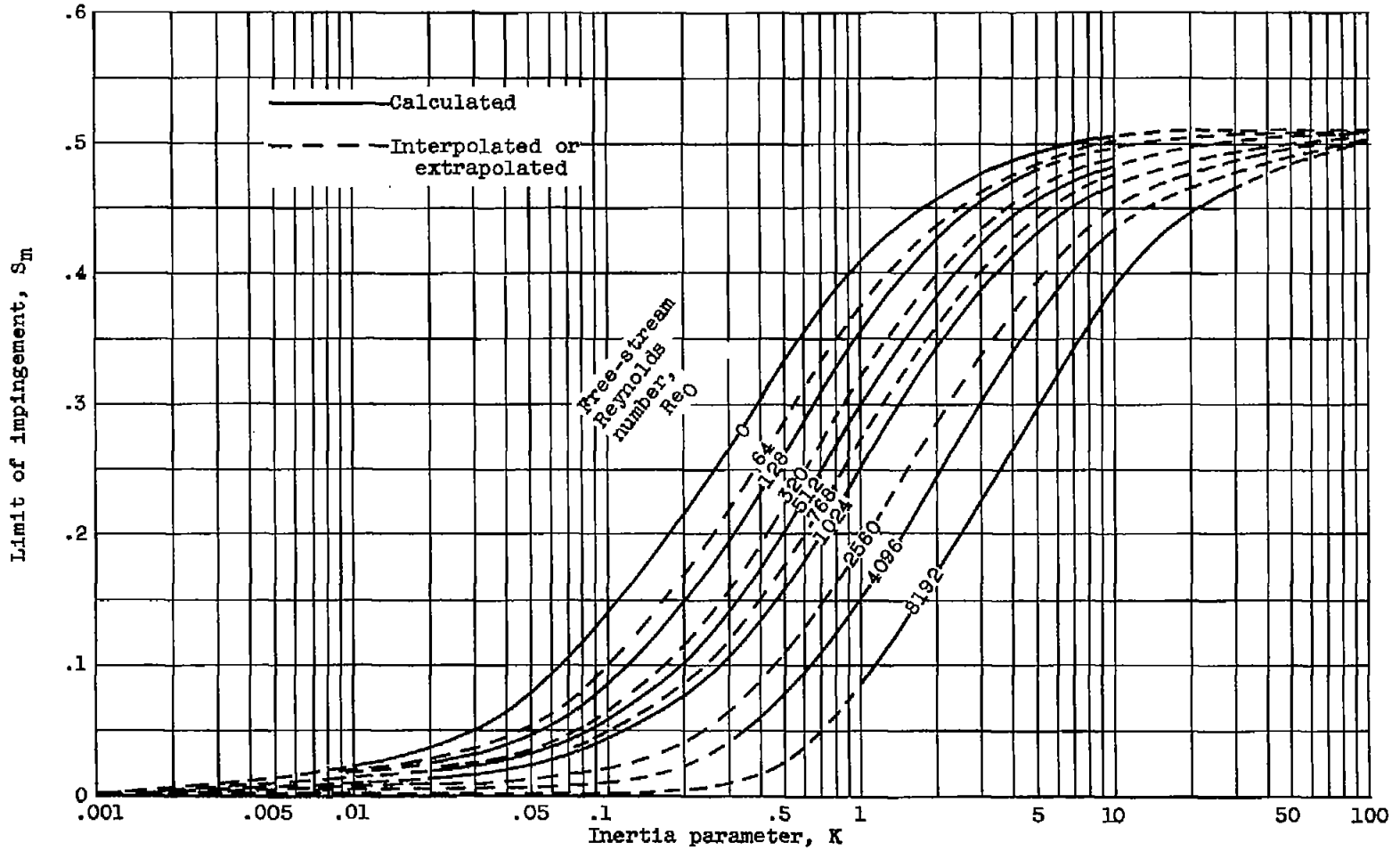
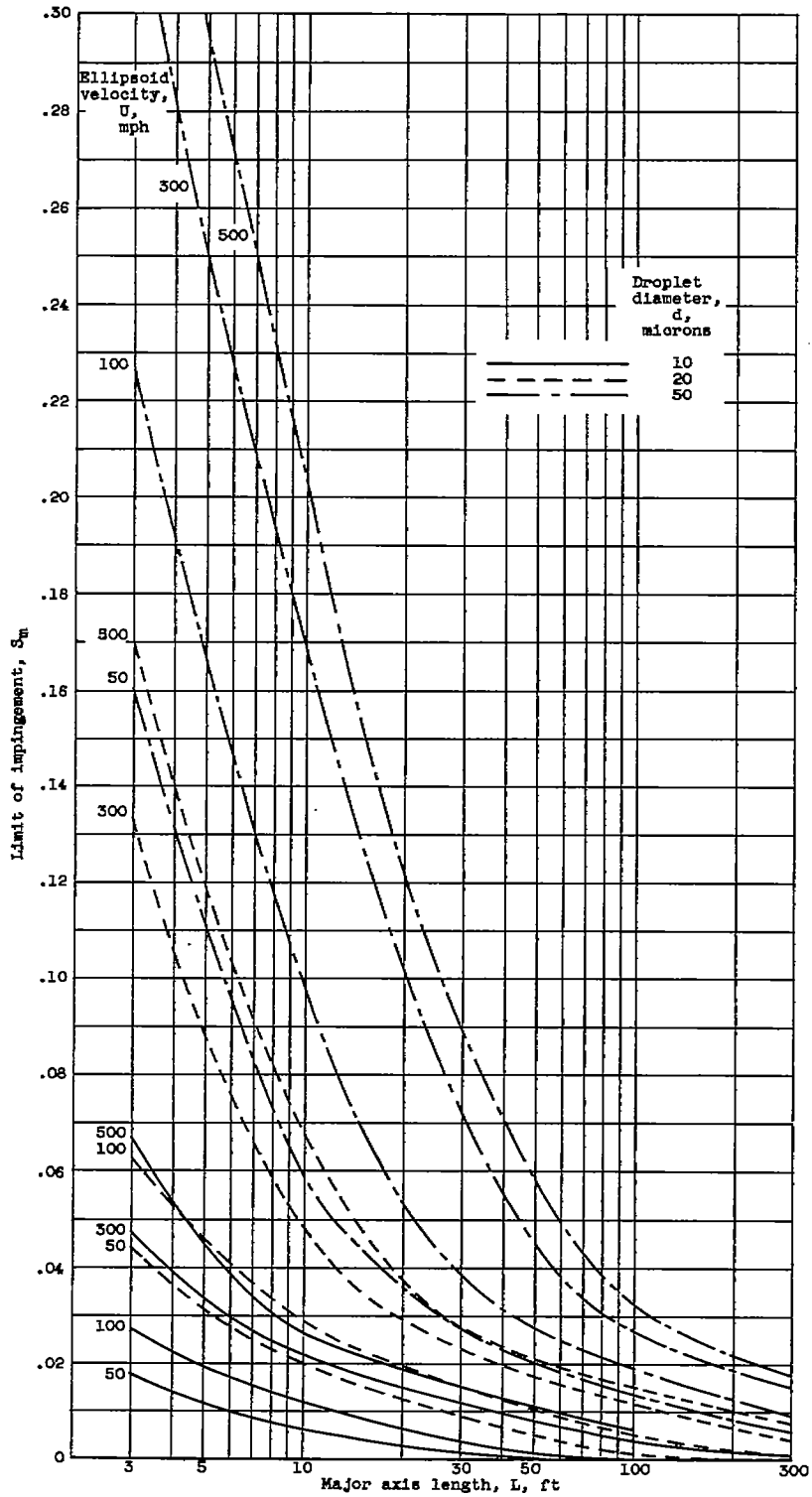


Figure 7. - Limit of impingement zone on surface of ellipsoid.

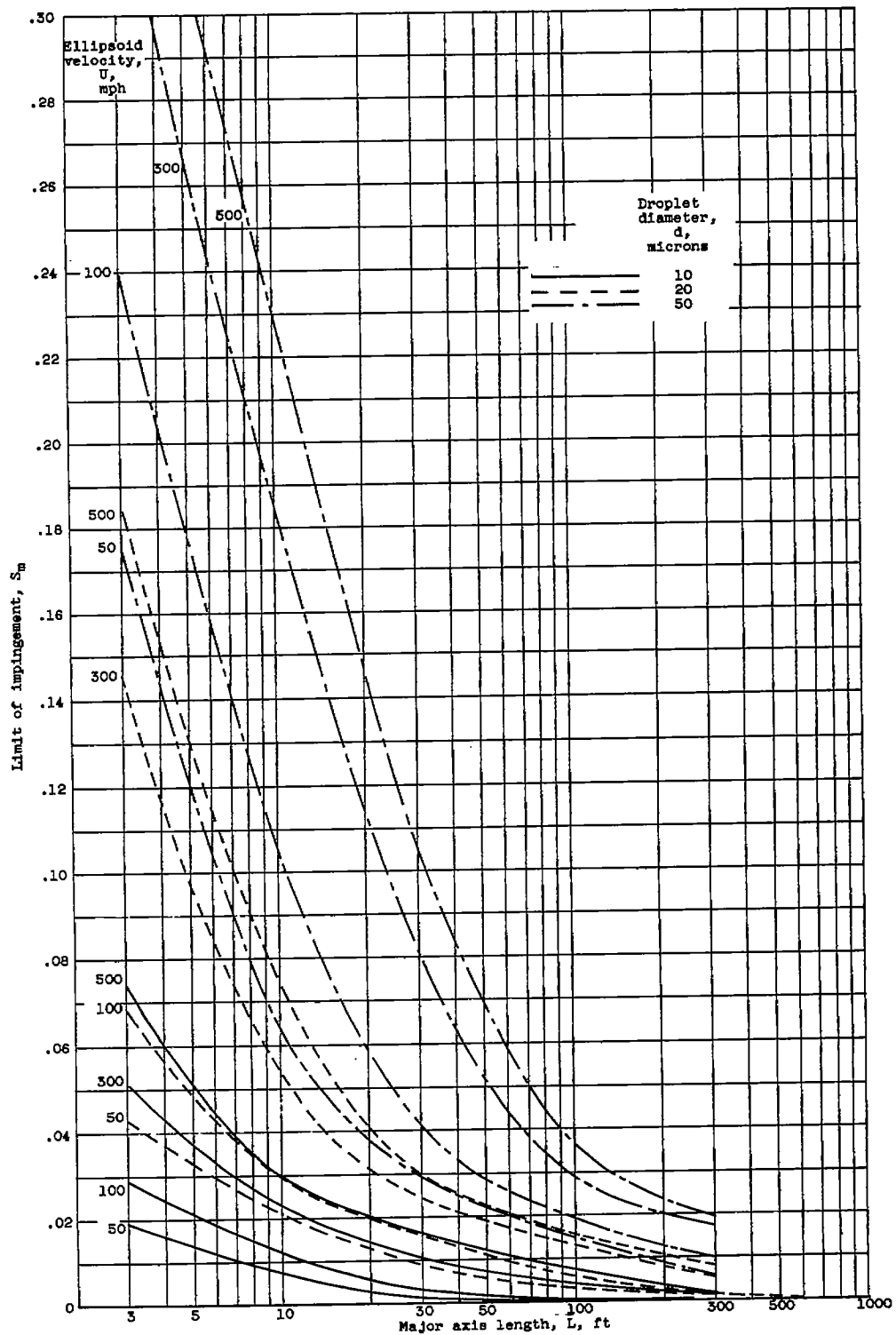
3217

CJ-4 back



(a) Pressure altitude, 5000 feet; temperature, 20° F.

Figure 8. - Maximum extent of impingement zone as function of major axis of ellipsoid.



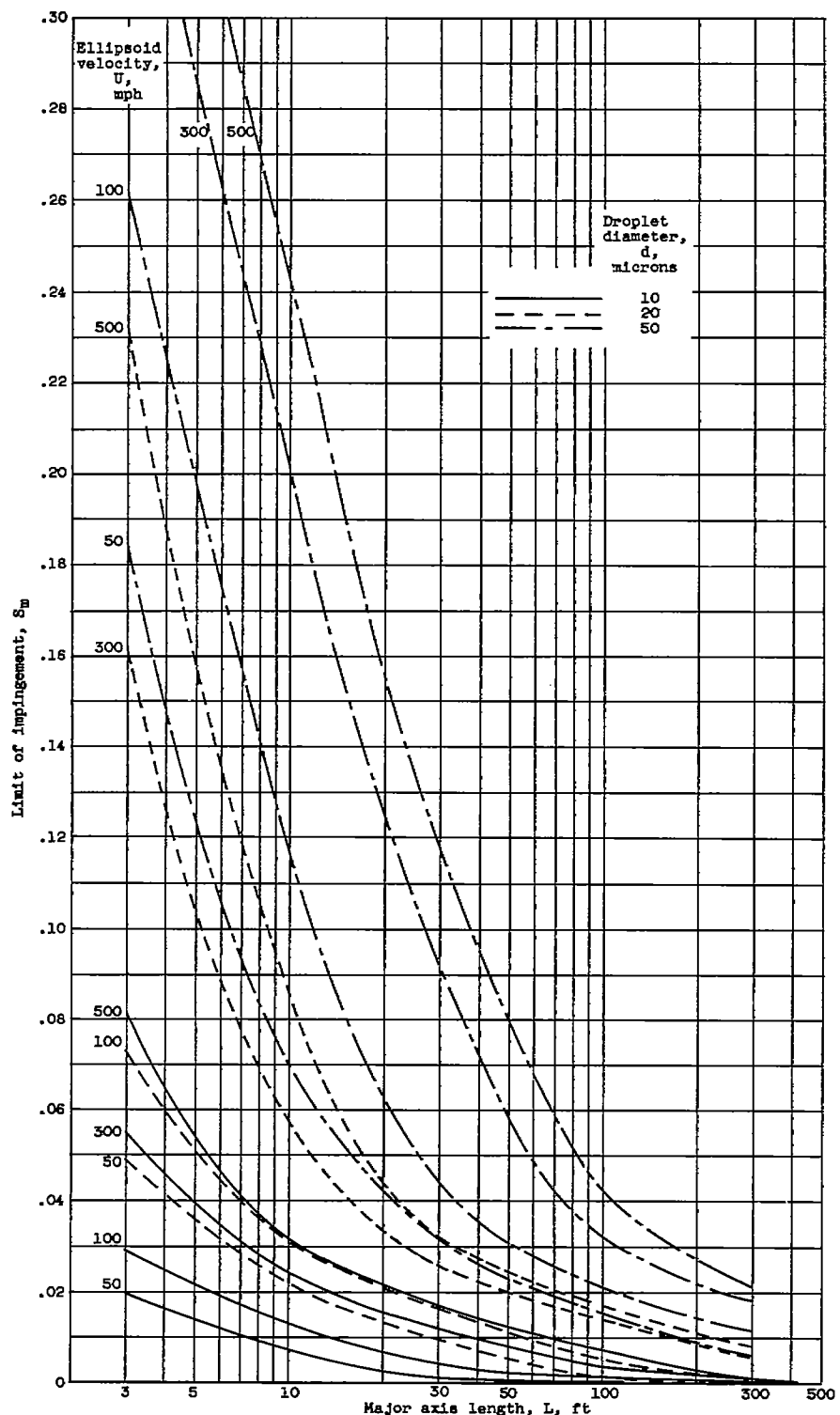
(b) Pressure altitude, 15,000 feet; temperature, 1° F.

Figure 8. - Continued. Maximum extent of impingement zone as function of major axis of ellipsoid.

3217

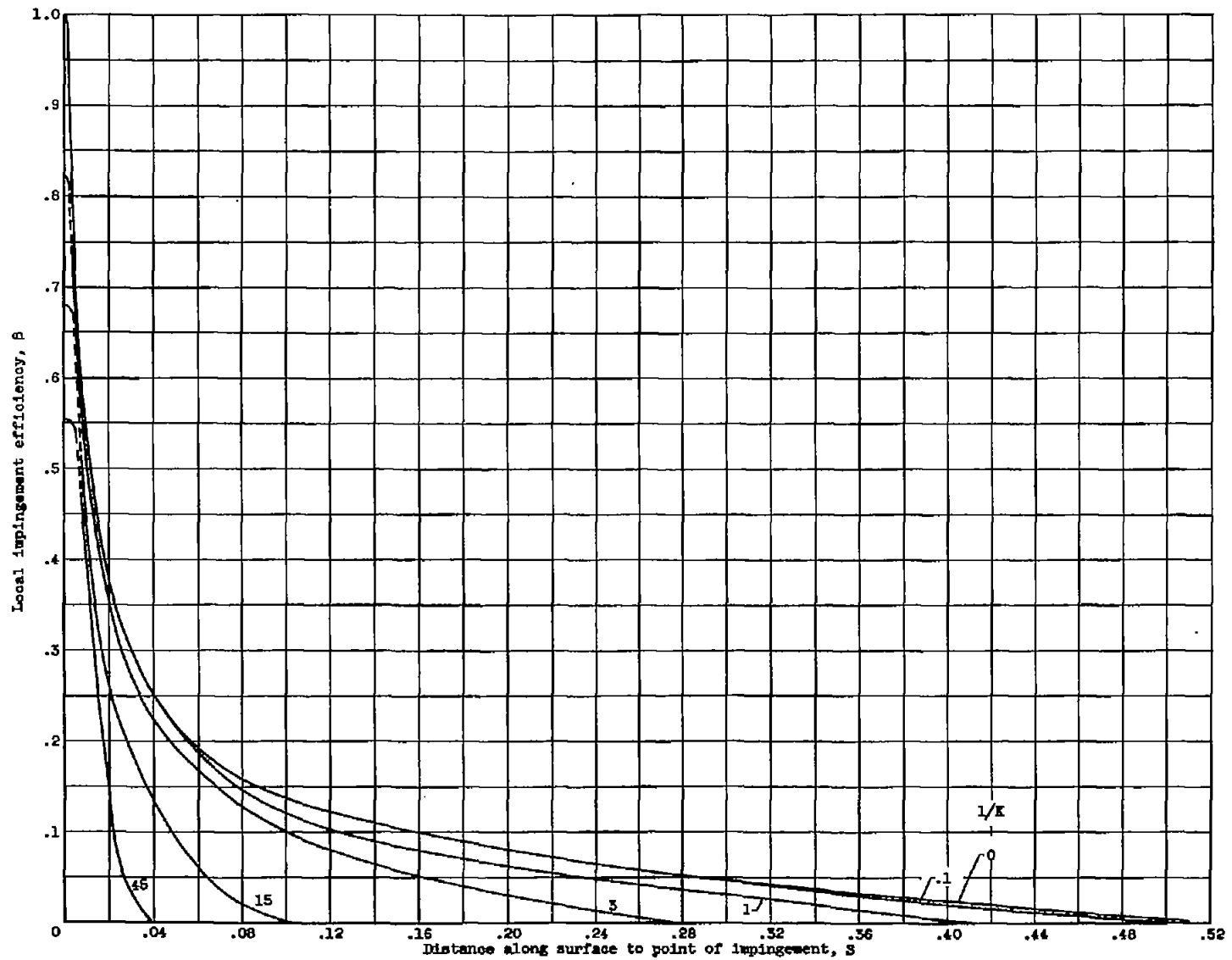


3217



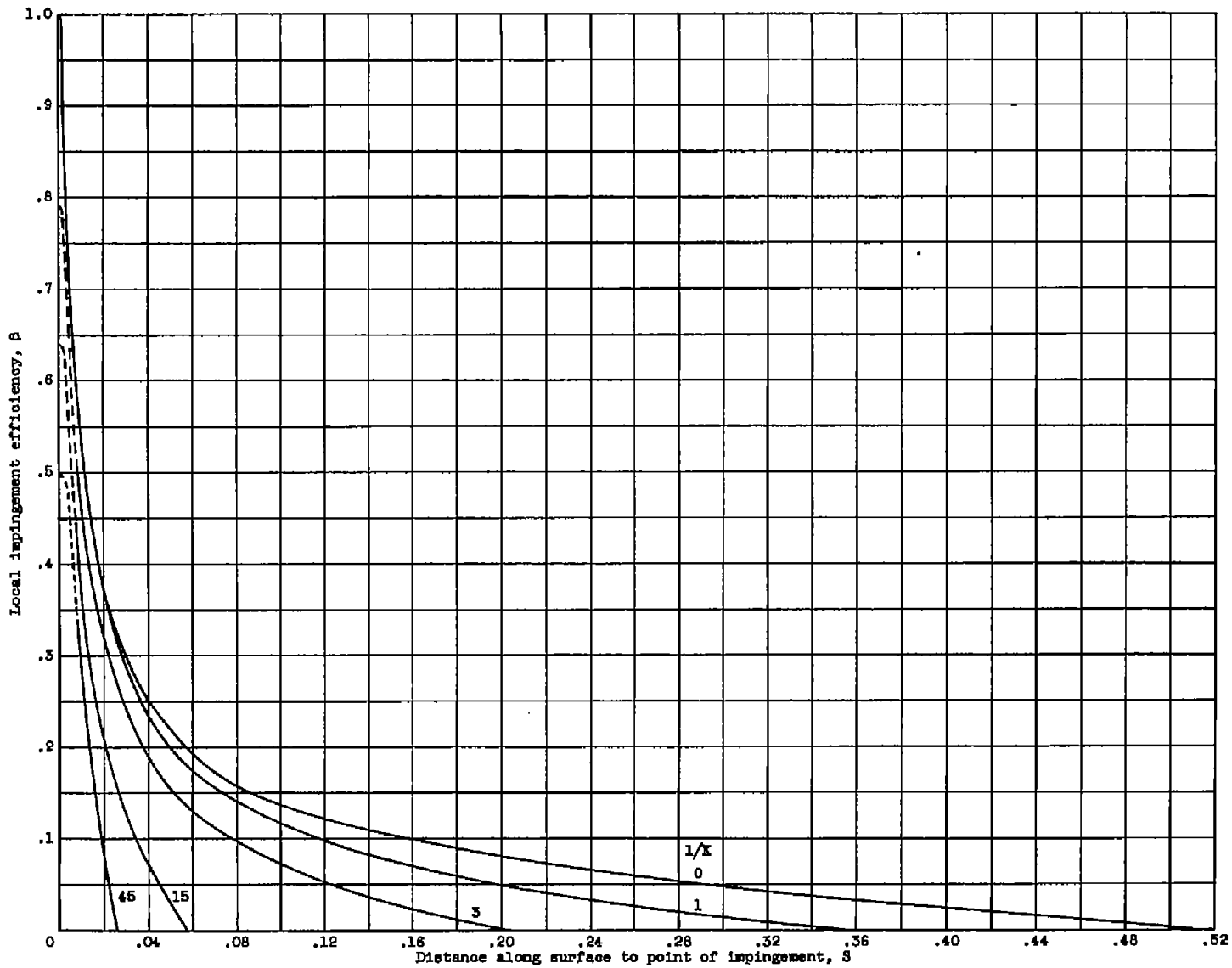
(c) Pressure altitude, 25,000 feet; temperature,  $-25^{\circ}$  F.

Figure 8. - Concluded. Maximum extent of impingement zone as function of major axis of ellipsoid.



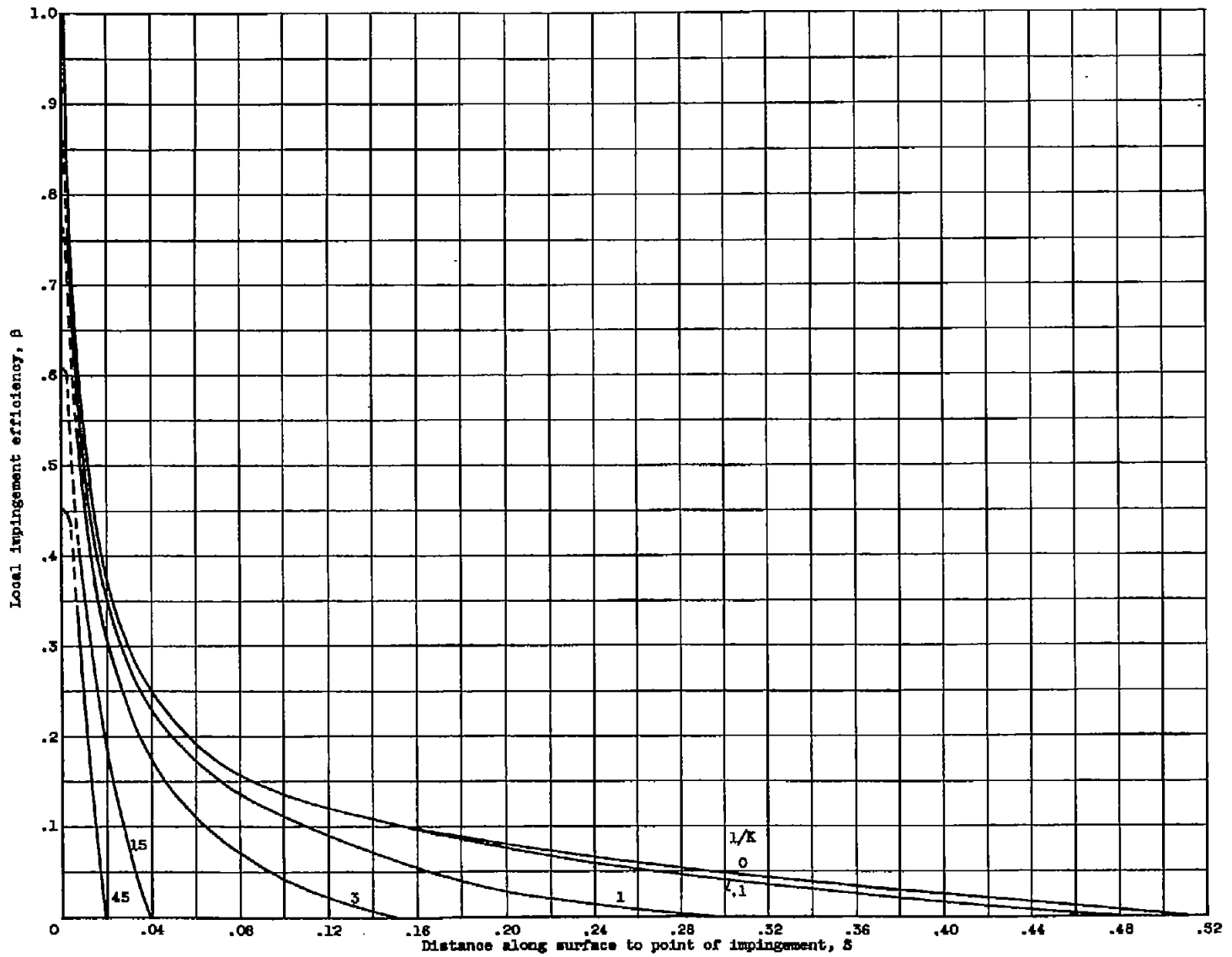
(a) Free-stream Reynolds number, 0.

Figure 9. - Local impingement efficiency:  $\beta = \frac{x_0}{r} \frac{dr_0}{ds}$ .



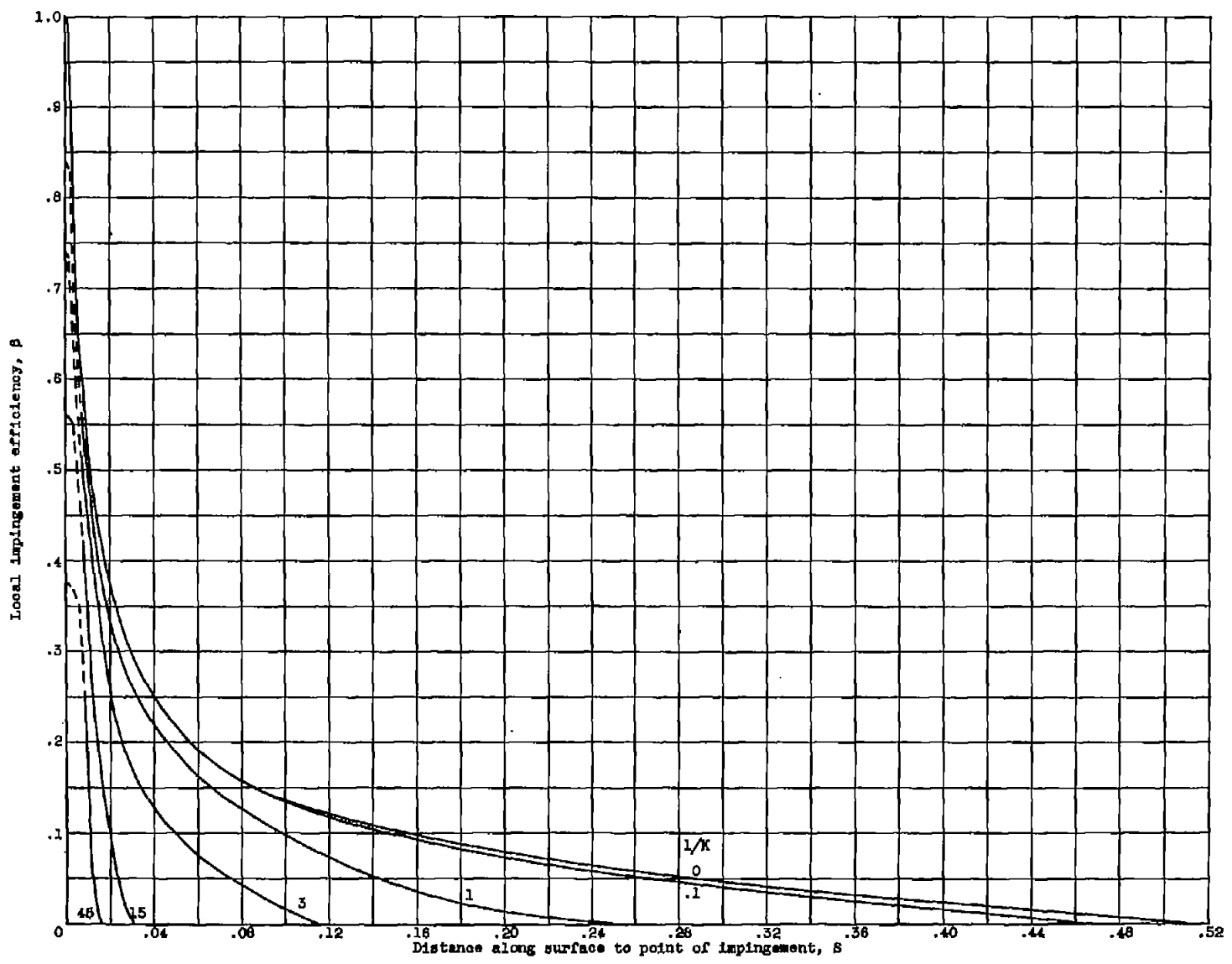
(b) Free-stream Reynolds number, 128.

Figure 9. - Continued. Local impingement efficiency:  $\beta = \frac{r_0}{r} \frac{dr_0}{dB}$ .



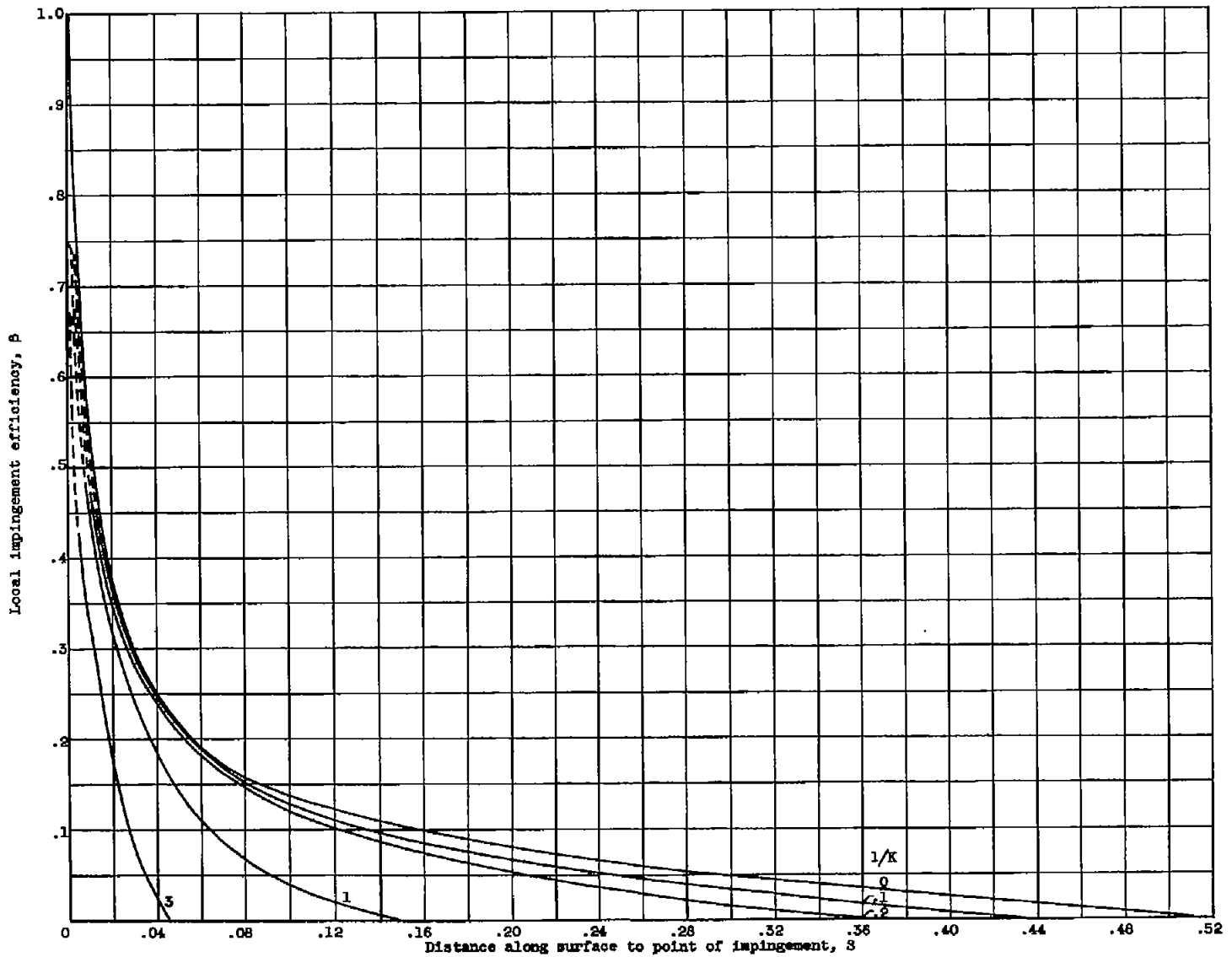
(c) Free-stream Reynolds number, 512.

Figure 9. - Continued. Local impingement efficiency:  $\beta = \frac{r_0}{r} \frac{dr_0}{ds}$ .



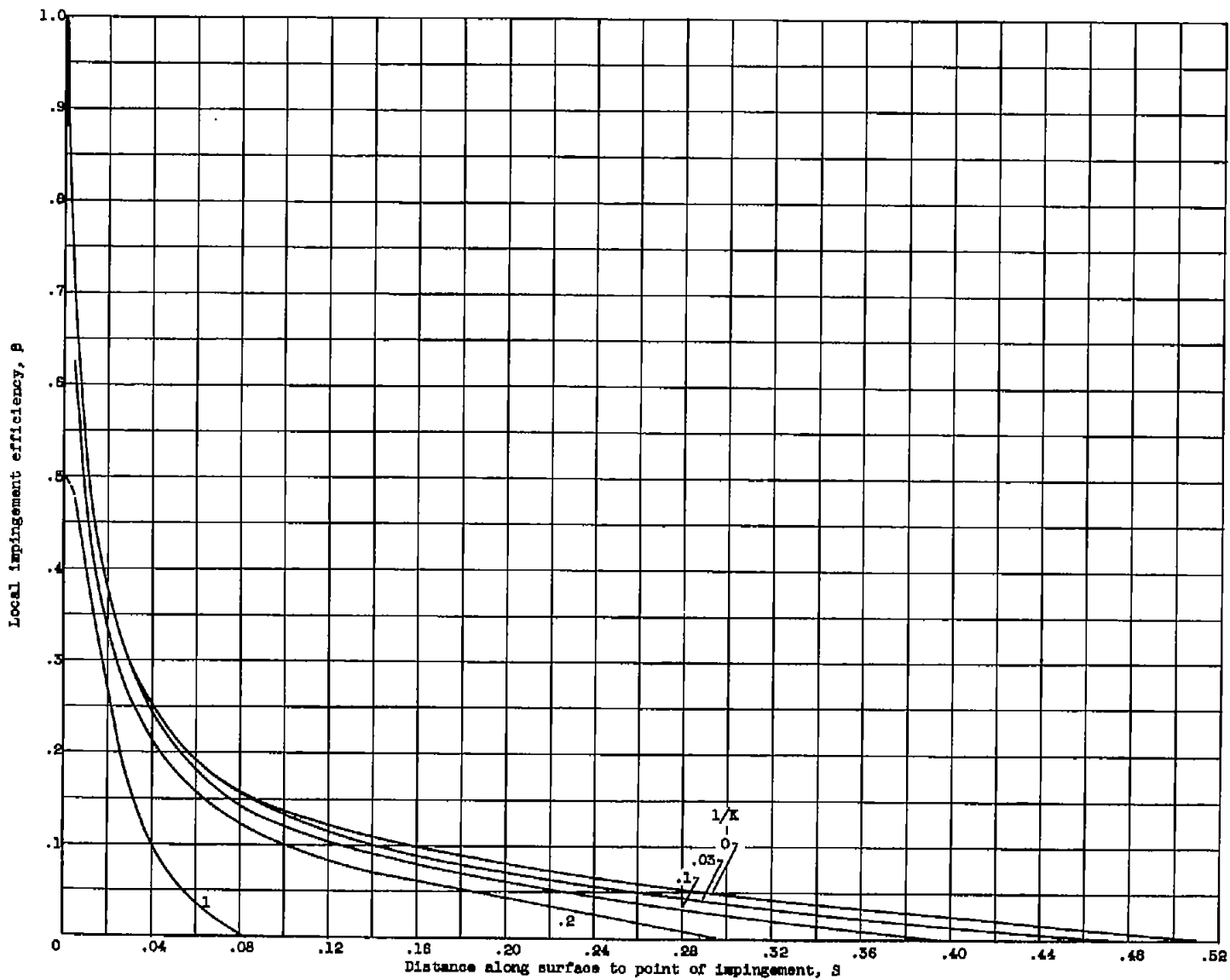
(d) Free-stream Reynolds number, 1024.

Figure 9. - Continued. Local impingement efficiency:  $\beta = \frac{r_0}{r} \frac{dr_0}{ds}$ .



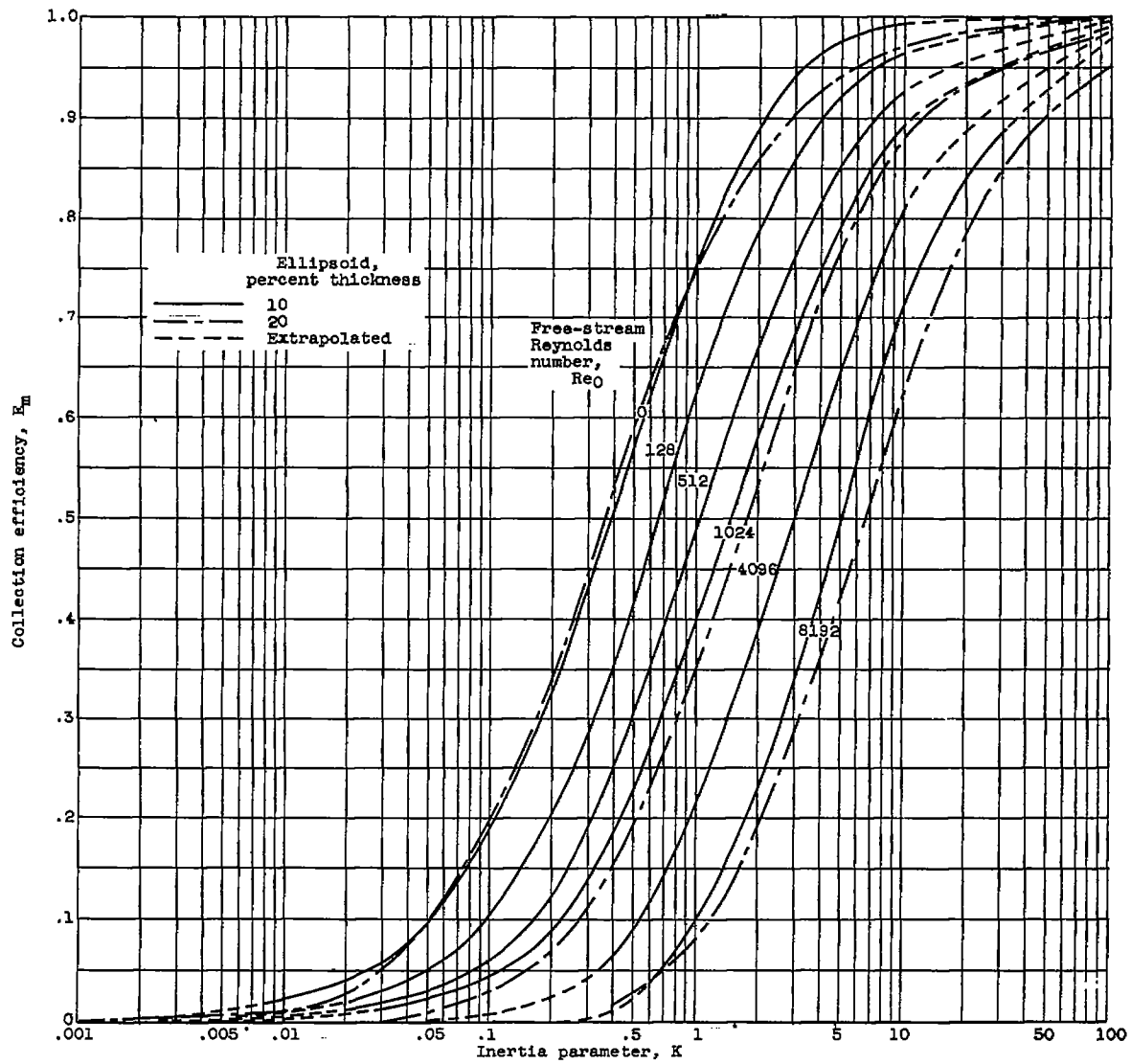
(a) Free-stream Reynolds number, 4098.

Figure 9. - Continued. Local impingement efficiency:  $\beta = \frac{r_0}{r} \frac{dr_0}{ds}$ .



( $r$ ) Free-stream Reynolds number, 8192.

Figure 8. - Concluded. Local impingement efficiency:  $\beta = \frac{r_0}{r} \frac{dr_0}{ds}$ .



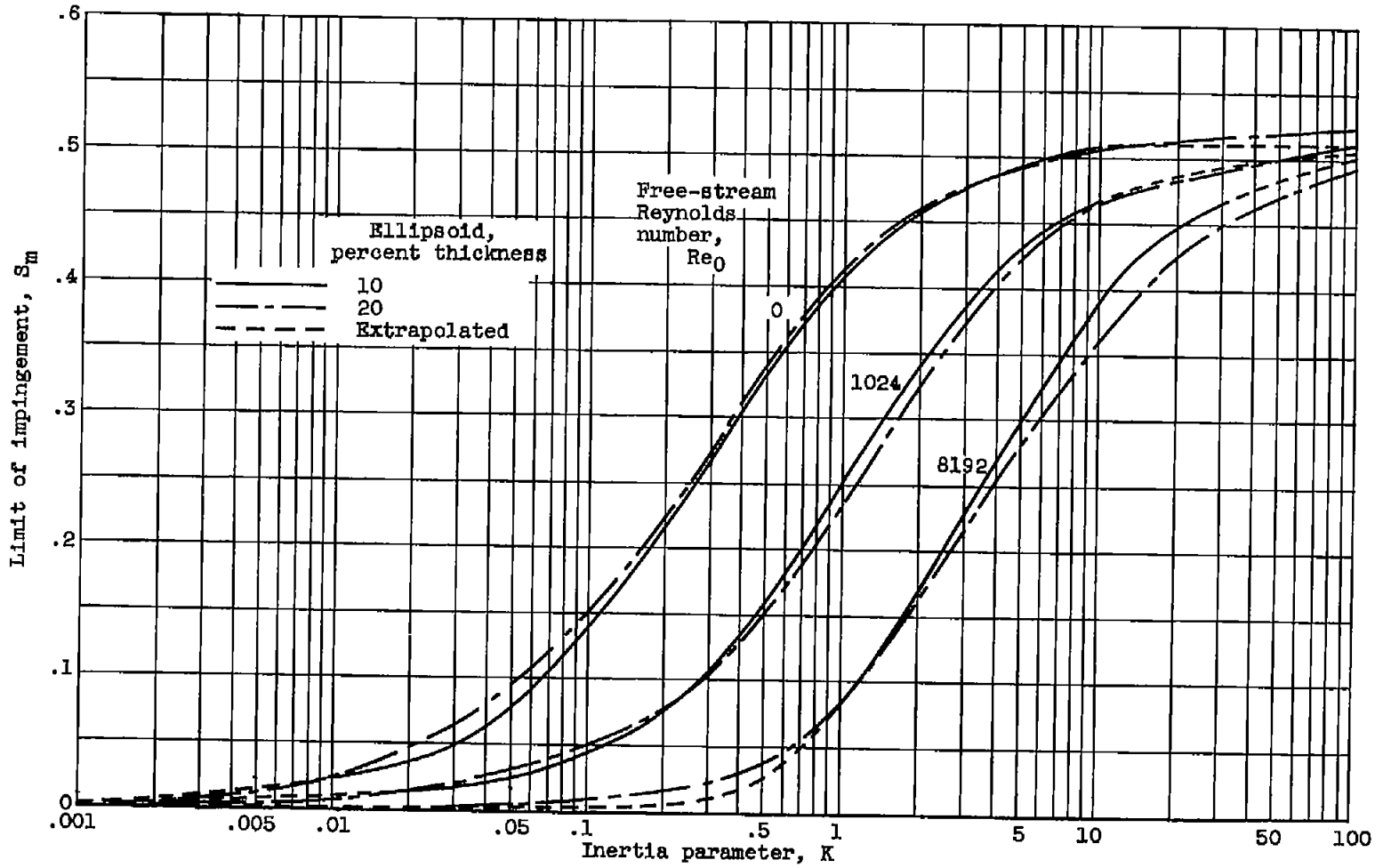
(a) Collection efficiency.

Figure 10. - Comparison of 10- and 20-percent-thick ellipsoids.



NACA-Tangley - 5-5-54 - 1000

NACA TN 3147



(b) Surface extent of impingement.

Figure 10. - Concluded. Comparison of 10- and 20-percent-thick ellipsoids.